Article
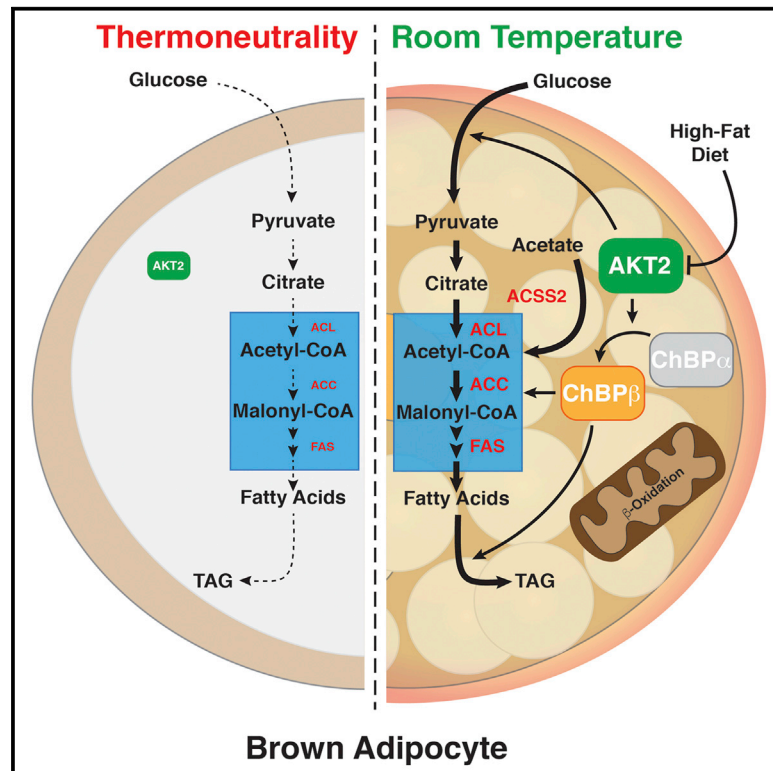
Brown Fat AKT2 Is a Cold-Induced Kinase that Stimulates ChREBP-Mediated *De Novo* Lipogenesis to Optimize Fuel Storage and Thermogenesis

Graphical Abstract

Authors

Joan Sanchez-Gurmaches,
Yuefeng Tang,
Naja Zenius Jespersen, ...,
Søren Nielsen, Camilla Scheele,
David A. Guertin

Correspondence

david.guertin@umassmed.edu

In Brief

Sanchez-Gurmaches et al. reveal a mechanism by which AKT signaling and metabolism intersect through ChREBP in brown fat to simultaneously promote lipid synthesis and oxidation, a paradoxical and poorly understood feature of thermogenesis. This pathway is required for optimum brown fat function and conserved in humans.

Highlights

- Mild cold profoundly induces *de novo* lipogenesis and lipid remodeling in BAT

- Lipogenesis is driven by ChREBP and requires AKT2, which is also induced by mild cold

- AKT2 is not required in BAT to maintain euthermia, but its loss enhances WAT browning

- High *ChREBPβ* and *Fasn* expression correlate with high *Ucp1* in human brown fat

CellPress

CellPress

Brown Fat AKT2 Is a Cold-Induced Kinase that Stimulates ChREBP-Mediated *De Novo* Lipogenesis to Optimize Fuel Storage and Thermogenesis

Joan Sanchez-Gurmaches,[1] Yuefeng Tang,[1] Naja Zenius Jespersen,[2,3] Martina Wallace,[4] Camila Martinez Calejman,[1] Sharvari Gujja,[1] Huawei Li,[1] Yvonne J.K. Edwards,[1] Christian Wolfrum,[5] Christian M. Metallo,[4] Søren Nielsen,[2] Camilla Scheele,[2,3] and David A. Guertin[1,6,*]

[1]Program in Molecular Medicine, University of Massachusetts Medical School, Worcester, MA 01605, USA
[2]The Centre of Inflammation and Metabolism and the Centre for Physical Activity Research, Rigshospitalet, University of Copenhagen, Copenhagen, Denmark
[3]Novo Nordisk Foundation Center for Basic Metabolic Research, University of Copenhagen, 2200 Copenhagen, Denmark
[4]Department of Bioengineering, University of California, San Diego, La Jolla, CA 92093, USA
[5]Institute of Food, Nutrition and Health, ETH-Zürich, Schorenstrasse 16, 8603 Schwerzenbach, Switzerland
[6]Lead Contact
*Correspondence: david.guertin@umassmed.edu
https://doi.org/10.1016/j.cmet.2017.10.008

SUMMARY

Brown adipose tissue (BAT) is a therapeutic target for metabolic diseases; thus, understanding its metabolic circuitry is clinically important. Many studies of BAT compare rodents mildly cold to those severely cold. Here, we compared BAT remodeling between thermoneutral and mild-cold-adapted mice, conditions more relevant to humans. Although BAT is renowned for catabolic β-oxidative capacity, we find paradoxically that the anabolic *de novo* lipogenesis (DNL) genes encoding ACLY, ACSS2, ACC, and FASN were among the most upregulated by mild cold and that, in humans, DNL correlates with *Ucp1* expression. The regulation and function of adipocyte DNL and its association with thermogenesis are not understood. We provide evidence suggesting that AKT2 drives DNL in adipocytes by stimulating ChREBPβ transcriptional activity and that cold induces the AKT2-ChREBP pathway in BAT to optimize fuel storage and thermogenesis. These data provide insight into adipocyte DNL regulation and function and illustrate the metabolic flexibility of thermogenesis.

INTRODUCTION

Brown adipose tissue (BAT) generates heat by an adaptive process called non-shivering thermogenesis, which requires an abundant fuel supply and the expression of uncoupling protein 1 (UCP1) (Cannon and Nedergaard, 2004). BAT allows rodents to maintain euthermia at temperatures below their thermoneutral (TN) zone (Cannon and Nedergaard, 2004). Human infants also have interscapular and perirenal BAT deposits, and about a decade ago it became apparent that BAT is present in adults.

In adult humans, BAT is located mainly in cervical, supraclavicular, paravertebral, and perirenal depots (Cypess et al., 2009; Nedergaard et al., 2007; Saito et al., 2009; van Marken Lichtenbelt et al., 2009; Virtanen et al., 2009), contributes to metabolic homeostasis (Hanssen et al., 2015; Ouellet et al., 2012), and may protect against obesity (Yoneshiro et al., 2011a, 2011b, 2013). This rationalized development of preclinical models to test the idea that stimulating BAT thermogenesis is a viable therapy to treat obesity (Harms and Seale, 2013). Thus, understanding the metabolic circuitry that drives BAT activity now has clinical implications.

BAT thermogenesis is stimulated by β-adrenergic receptor (AR) signaling principally through the β3-AR in rodents. Norepinephrine, or a β3 agonist such as CL316,243, stimulates production of cAMP, which activates protein kinase A (PKA) to drive transcription of thermogenic genes (including *ucp1*) and lipolysis (Cannon and Nedergaard, 2004). Free fatty acids (FAs) activate UCP1 (Fedorenko et al., 2012) and provide initial fuel for FA oxidation (Cannon and Nedergaard, 2004). Circulating exogenous FA and glucose provide additional fuel for catabolism during prolonged cold (Bartelt et al., 2011; Labbe et al., 2015, 2016), which is the basis for tracers of BAT activity such as ^{18}F-FDG (Cypess et al., 2009; Saito et al., 2009; van Marken Lichtenbelt et al., 2009; Virtanen et al., 2009). Less appreciated is that active BAT also engages the anabolic *de novo* lipogenesis (DNL) pathway (McCormack and Denton, 1977; Mottillo et al., 2014; Shimazu and Takahashi, 1980; Townsend and Tseng, 2015; Trayhurn, 1979; Yu et al., 2002), which seems paradoxical in light of the fact that FA synthesis and FA oxidation can antagonize each other in other tissues (Hue and Taegtmeyer, 2009). However, the regulation and function of DNL in cold-induced BAT remodeling is largely unexplored.

Therapeutically stimulating thermogenesis could be transformative for people suffering from metabolic syndrome, obesity, type 2 diabetes, and cardiovascular disease (Hanssen et al., 2015; Ouellet et al., 2012; Yoneshiro et al., 2011a, 2011b, 2013). It is debated as to whether human adult thermogenic cells are classic brown adipocytes, as in newborns, or brite/beige
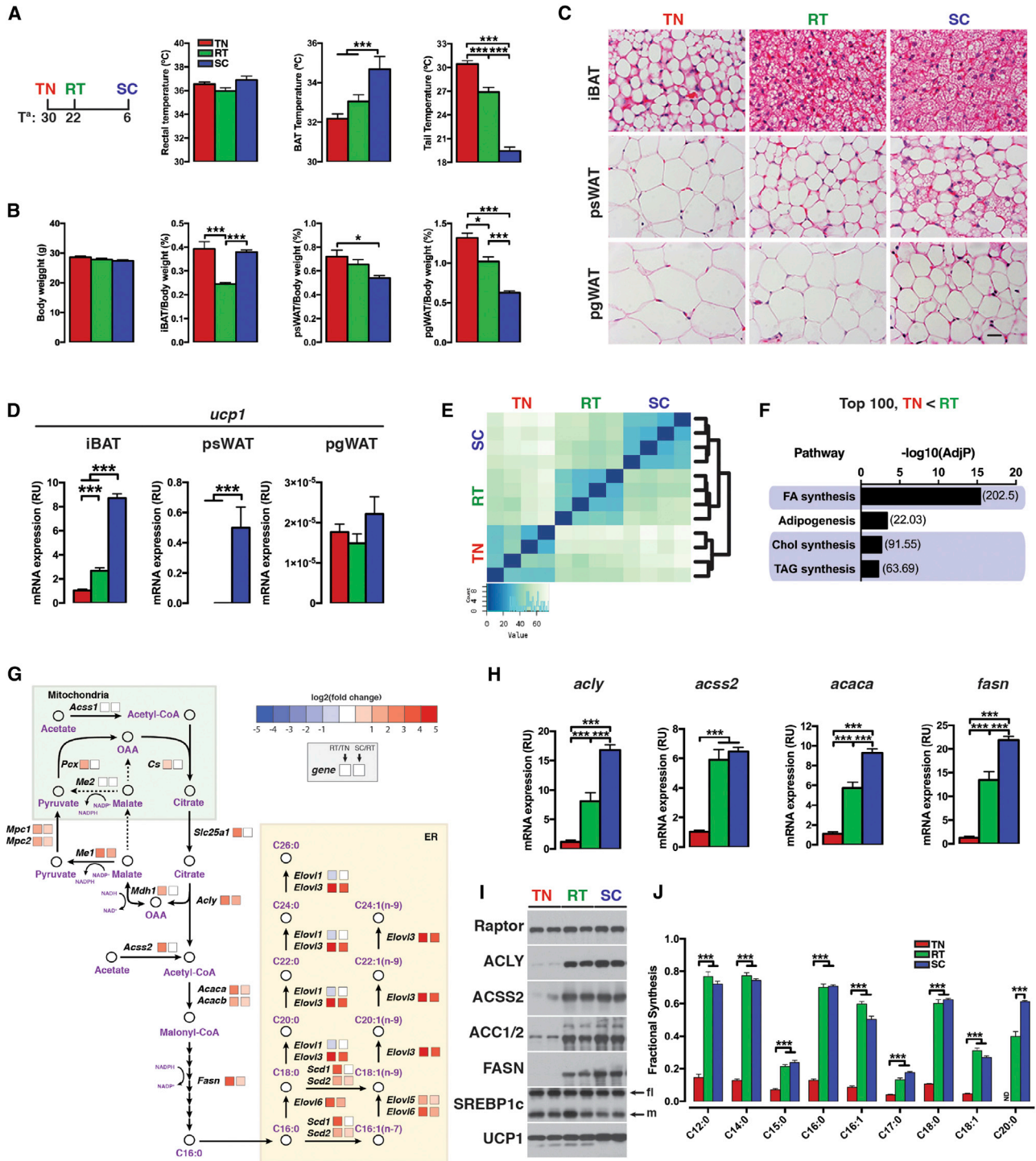
Figure 1. Profound BAT Remodeling Is Induced by Mild Cold and Strongly Associates with Increased Anabolic *De Novo* Lipid Synthesis

(A) Environmental temperatures and rectal, BAT, and tail temperatures recorded at in random fed C57BL/6J mice (n = 6).

(B) Total body and fat depot weights of C57BL/6J mice adapted to the indicated temperatures (n = 20).

(C) Representative H&E images of fat depots from C57BL/6J mice adapted to the indicated temperatures. Scale bar, 100 μm.

(D) qRT-PCR analysis of *ucp1* mRNA levels from the fat depots of C57BL/6J mice adapted to the indicated temperatures (n = 8). The y axis for each is normalized to TN iBAT.

(E) RNA-seq-based clustering of iBAT samples from C57BL/6J mice adapted to the indicated temperatures (n = 4).

(F) Pathway analysis of the top 100 most upregulated genes in RT iBAT versus TN (n = 4). AdjP, adjusted p value. Category ratio of enrichment (R, observed number of genes in the category versus expected) is shown in brackets.

adipocytes, which exist in subcutaneous fat and interconvert between a brown and white adipocyte-like state upon stress (Rosenwald et al., 2013; Shinoda et al., 2015; Townsend and Tseng, 2015; Xue et al., 2015); mice have both (Sanchez-Gurmaches et al., 2016). Rodent brite/beige adipocytes share some markers with classical brown adipocytes in humans (Jespersen et al., 2013). However, studies using rodents often compare subcutaneous white adipose tissue (WAT) (and BAT) between animals housed at standard mouse facility temperature (often 21°C–22°C) and severe cold (SC) (typically 4°C–10°C), which induces "browning" of WAT, but also exposes mice to extreme conditions that may not be physiologically relevant to humans (Cannon and Nedergaard, 2011; Sanchez-Gurmaches et al., 2016). In fact, mice living at 22°C are already cold because this temperature is below their (TN) zone, which profoundly impacts their basal metabolic rate (Cannon and Nedergaard, 2011). When living without thermal stress, mouse metabolism is more "humanized," and their BAT deposits adopt WAT-like characteristics (Cannon and Nedergaard, 2011; Sanchez-Gurmaches et al., 2016). This raises an interesting question as to whether the interconversion of classic BAT between inactive and active states under mild cold is a better model of human thermogenic adipocytes.

Because fewer studies of BAT analyze the transition between no thermal stress and mild cold, we hypothesized that overemphasis on experiments performed in continuously cold stressed mice has led to an underappreciation of certain adaptive features of BAT metabolic reprogramming that could be relevant to humans. To test this, we comparatively analyzed the gene expression and lipid remodeling that occurs in the BAT of mice adapted to thermoneutrality (30°C), mild cold (22°C), and SC (4°C). We find that the anabolic DNL pathway, globally, is one of the most upregulated pathways even by mild cold, and that AKT2 signaling, which classically antagonizes PKA signaling by reducing cAMP levels (Kitamura et al., 1999), appears to cooperate with PKA signaling under these conditions to drive DNL genes. Mechanistically, AKT2 stimulates DNL by driving ChREBP transcriptional activity, which is required in BAT for fuel storage, but dispensable for thermogenic gene expression and maintaining euthermia in the cold. However, without BAT AKT2, more brite/beige adipocytes are recruited to subcutaneous WAT upon prolonged cold exposure, indicating that AKT2 is required for optimum BAT function. These findings have important implications for understanding BAT remodeling under human-relevant environmental conditions, how AKT functions in adipose tissue, and the remarkable metabolic flexibility of BAT that allows it to defend body temperature at all costs.

RESULTS

Mild Cold Profoundly Remodels BAT Anatomy

Age-matched C56BL/6J male mice were adapted to TN (30°C), room temperature (RT) (22°C), or SC (6°C) for 28 days. Body temperature is constant across conditions, while BAT surface temperature increases and tail temperature decreases, confirming higher thermal dissipation at lower temperatures (Figures 1A and S1A). Total body weight is unaffected (Figure 1B); however, the BAT mass (i.e., interscapular, subscapular, and cervical) is larger in TN-housed mice (Figures 1B and S1B). The increase is due to hypertrophy indicated by a switch in lipid droplet number and size from being small and multilocular at RT to large and unilocular at TN (Figures 1C and S1C). Total BAT mass also increases upon adaptation to SC (Figures 1B and S1B), but by cell hyperplasia as cell size is unchanged and lipid droplets remain small and multilocular (Figures 1C and S1C). In comparison, posterior subcutaneous WAT (psWAT) and perigonadal visceral WAT (pgWAT) mass is largest at TN, and both depots progressively decrease in size with temperature (Figure 1B). White adipocytes size also decreases with temperature; however, in the psWAT most adipocytes are unilocular at TN and RT, while large numbers of multilocular adipocytes called brown-like in white (i.e., "brite" also known as beige) adipocytes appear upon adaptation to SC. In contrast, the pgWAT adipocytes remain unilocular under all conditions (Figure 1C). In BAT, *ucp1* mRNA increases with cold temperature (Figure 1D). In psWAT, *ucp1* expression only increases dramatically upon SC acclimation (Figure 1D); however, the *ucp1* levels remain magnitudes lower than in BAT (Figure 1D). The *ucp1* levels in pgWAT are barely detectable and do not respond to temperature (Figure 1D). Thus, in response to mild cold, dramatic transformation between WAT-like and active BAT characteristics occurs in the classic brown fat depots, and similar transformations are only seen in psWAT on a lesser scale under extreme cold stress.

Mild Cold Globally Induces DNL Genes in BAT

Clustering of RNA sequencing (RNA-seq) data indicates that BAT gene expression is more diverged between TN and RT (a range of 8°C) than between RT and SC (a 16°C difference) (Figure 1E). A total of 1,994 genes are upregulated in BAT by mild cold (false discovery rate [FDR] < 0.05) and a full description of the changes is available in Table S1 (RNA-seq and lipidomics data related to Figure 1). Of genes increasing expression, many function in FA oxidation, the electron transport chain, oxidative phosphorylation, and the tricarboxylic acid (TCA) cycle (Figure S1D), which is not surprising given the well-known lipid catabolic activity of active BAT. However, for most of these genes the magnitude of induction is relatively modest (Figure S1E). In contrast, an analysis of the top 100 genes most upregulated by mild cold (FDR < 0.05) reveals that DNL, cholesterol synthesis, and triacylglyceride (TG) synthesis genes are over-represented (Figure 1F). This highlights an interesting paradox; in active BAT, which is best known for its catabolically high FA oxidation (Bartelt et al., 2011; Cannon and Nedergaard, 2004; Labbe et al., 2015, 2016), anabolic *de novo* FA synthesis pathways, which often antagonize FA oxidation (Hue and Taegtmeyer, 2009) are globally among the most highly upregulated pathways.

(G) The *de novo* lipogenesis pathway. Gene expression changes are indicated in the boxes to the right of each gene name.

(H) qRT-PCR analysis on iBAT samples from C57BL/6J mice adapted to TN, RT and SC (n = 8).

(I) Western blots on iBAT samples from C57BL/6J mice.

(J) D2O labeling showing the fraction of newly synthesized FA species over 3 days in the iBAT of C57BL/6J mice at each temperature (n = 6).

Bar graphs represent mean ± SEM. *p < 0.05, ***p < 0.001. See also Figure S1.

Previous studies recognized an association between lipogenesis and BAT activity (McCormack and Denton, 1977; Mottillo et al., 2014; Shimazu and Takahashi, 1980; Townsend and Tseng, 2015; Trayhurn, 1979; Yu et al., 2002); however, its functional significance has been unclear. Among the lipogenic genes most upregulated by mild cold (relative to TN) are *ATP-citrate lyase* (*Acly;* 8.1-fold), *acyl-CoA synthetase short chain family member 2* (*Acss2;* 5.9-fold), *acetyl-CoA carboxylase* (*Acaca;* 5.7-fold), and *fatty acid synthase* (*Fasn;* 13.5-fold). This was confirmed by qRT-PCR (Figures 1G and 1H) and western blot, which shows a striking increase in total protein (Figure 1I). ACLY and ACSS2 generate cytoplasmic acetyl-CoA for *de novo* FA synthesis; ACLY from mitochondria-exported citrate, and ACSS2 from acetate (Figure 1G). In contrast, expression *Acss1*, which encodes a mitochondrial matrix acetyl-CoA synthetase with high specificity for acetate does not significantly change with mild cold (Figures 1G and S1F). ACLY, ACC, and FASN increase only slightly more with SC, and ACSS2 is unchanged (Figures 1G–1I), indicating DNL enzymes are near maximally expressed in mild cold.

Several DNL support genes also increase in the BAT with mild cold, including the mitochondrial citrate transporter *(Slc25a1)*, cytoplasmic malic enzyme (*Me1*), which encodes a decarboxylase that converts malate to pyruvate to regenerate NADPH for FA synthesis, and *Mpc1* and *Mpc2*, whose products form a heterodimer that transports pyruvate into the mitochondria (Figure 1G). Many glucose handling (e.g., glycolysis) enzymes are also elevated (Figure S1D), including the glucose/fructose transporter *Slc2a5 (Glut5)*, suggesting a role for fructose as a thermogenic fuel, and *Gck (glucokinase),* which increases 22-fold (Figure S2B). *Gck* is interesting because, unlike hexokinase, its activity is driven by glucose levels, it is not inhibited by glucose-6-phosphate, and it is thought to be liver and pancreas specific (Purich et al., 1973). Downstream lipid-processing enzymes, including stearoyl-CoA desaturase (*Scd1*), elongation of very long chain FA protein 6 (*Elovl6*), and *Elovl3* (a gene known to increase in BAT with SC) also increase with mild cold (Figure 1G). Consistently, there is a large increase in the abundance of *de novo* synthesized FA in cold-acclimated BAT by *in vivo* D_2O labeling (Figure 1J). All examined FA species displayed upregulated D_2O enrichment with mild cold ranging from 3.1- to 7.2 depending on the FA species, and did not increase further with SC except for C20:0 FA, which was undetectable at TN (Figure 1J). Thus, mild cold potently induces DNL in BAT.

Mild Cold Remodels the Global Lipid Landscape in BAT

Many TG synthesis-related genes also increase with mild cold (Figures 1F and S1D), but a few are particularly noteworthy. Firstly, *glycerol kinase* (*Gyk*) increases 2.3-fold (Figure S1G). In the liver, GYK phosphorylates glycerol as an alternative route (from the DHAP dehydrogenation pathway) to making glycerol-3-phosphate (G-3-P), the backbone for acylation during TG and glycerophospholipid biosynthesis. It was thought that adipocytes lack GYK (Steinberg et al., 1961), although this is controversial (Guan et al., 2002). Secondly, there is a switch in isoform expression levels for genes encoding 1-acylglycerol-3-phosphate O-acyltransferase (AGPAT) family members, which convert lysophosphatidic acid to phosphatidic acid in the first step of TG/phospholipid biosynthesis. For example, *Agpat2*

increases 4.4-fold, while *Agpat4* decreases 2.9-fold (Figure S1G). Thirdly, the *monoacylglycerol acyltransferase 1* (*Mogat1*) gene increases by 4.2-fold (Figure S1G). MOGAT1 catalyzes the conversion of monoacylglycerols to diacylglycerols (DGs) in a less-studied alternative to the G-3-P pathway for generating TGs (Hall et al., 2012).

The collective increases in both DNL and TG synthesis pathway genes suggests the global lipid landscape might also remodel with cold. Indeed, most lipid classes including TG, DG, PG, PI, PS, PE, PC, LPE, LPC, and SM (see figure legends for definitions) exhibit significant changes in their distribution in response to temperature (Figures 2A–2C and S3A; Table S1, RNA-seq and lipidomics data related to Figure 2). Intriguingly, ranking of 256 TG species, based on relative change between TN and RT, reveals a positive correlation between TN and having longer and more desaturated side chains (Figure 2D). On the other hand, changes in DGs between TN and RT conditions positively correlates with more desaturations only (Figure 2E), while phosphatidylethanolamine remodeling between TN and RT did not correlate with either (Figure 2F). Thus, cold temperature also remodels the lipid landscape in patterns that vary between lipid classes.

Lipogenic Enzyme Expression and Lipid Remodeling Requires AKT2

To better understand the signal(s) driving DNL, we examined the RNA-seq data for genes encoding signaling pathway components whose expression mirrored the DNL genes. This revealed insulin signaling as a pathway highly over-represented for genes elevated in mild cold (Figure 3A). In particular, the mRNA and protein levels of the insulin effector AKT2 is higher in mice living at RT compared with TN, and similar to DNL genes, there is little additional change upon further adaptation to SC (Figures 3B and 3C). In contrast, AKT1 shows no clear change (Figures 3B and 3C). The increase in AKT2 protein correlates with increased AKT2 phosphorylation (Figure 3C). This is interesting because PKA and AKT signaling are often antagonistic, leading us to hypothesize that cold stimulates DNL genes in BAT through an AKT2-dependent pathway that cooperates with PKA signaling to fuel BAT metabolism.

To investigate the role of AKT signaling in BAT DNL, we generated brown adipocyte-specific *Akt1* and *Akt2* knockout mice using a tamoxifen-inducible *Ucp1-Cre*[ERT2] driver (Rosenwald et al., 2013; Wan et al., 2011, 2012). We validated the efficiency and specificity of recombination by combining *Ucp1-Cre*[ERT2] with a Cre-driven membrane-targeted GFP reporter (Figure S4A). Three weeks after tamoxifen treatment, robust and specific recombination was detected in nearly all mature brown adipocytes examined and in no white adipocytes (Figure S4A). We next generated *Akt1*[Ucp1CreER] and *Akt2*[Ucp1CreER] mice living at RT and induced deletion at 6 weeks of age. At 3 weeks post deletion, *Akt1*[Ucp1CreER] mice do not have any measurable differences in body weight or individual tissue mass (Figure S4B). In contrast, *Akt2*[Ucp1CreER] mice have smaller iBAT, sBAT, and cBAT mass (Figure 3D). We ruled out tamoxifen effects by also deleting *Akt2* with a constitutive *Ucp1-Cre* driver, which results in the same phenotype (Figures S4C and S4D). Knockout was confirmed by western blot (Figure S4E). Deleting *Akt2* with either Cre decreases the total amount of pan-Akt-T308
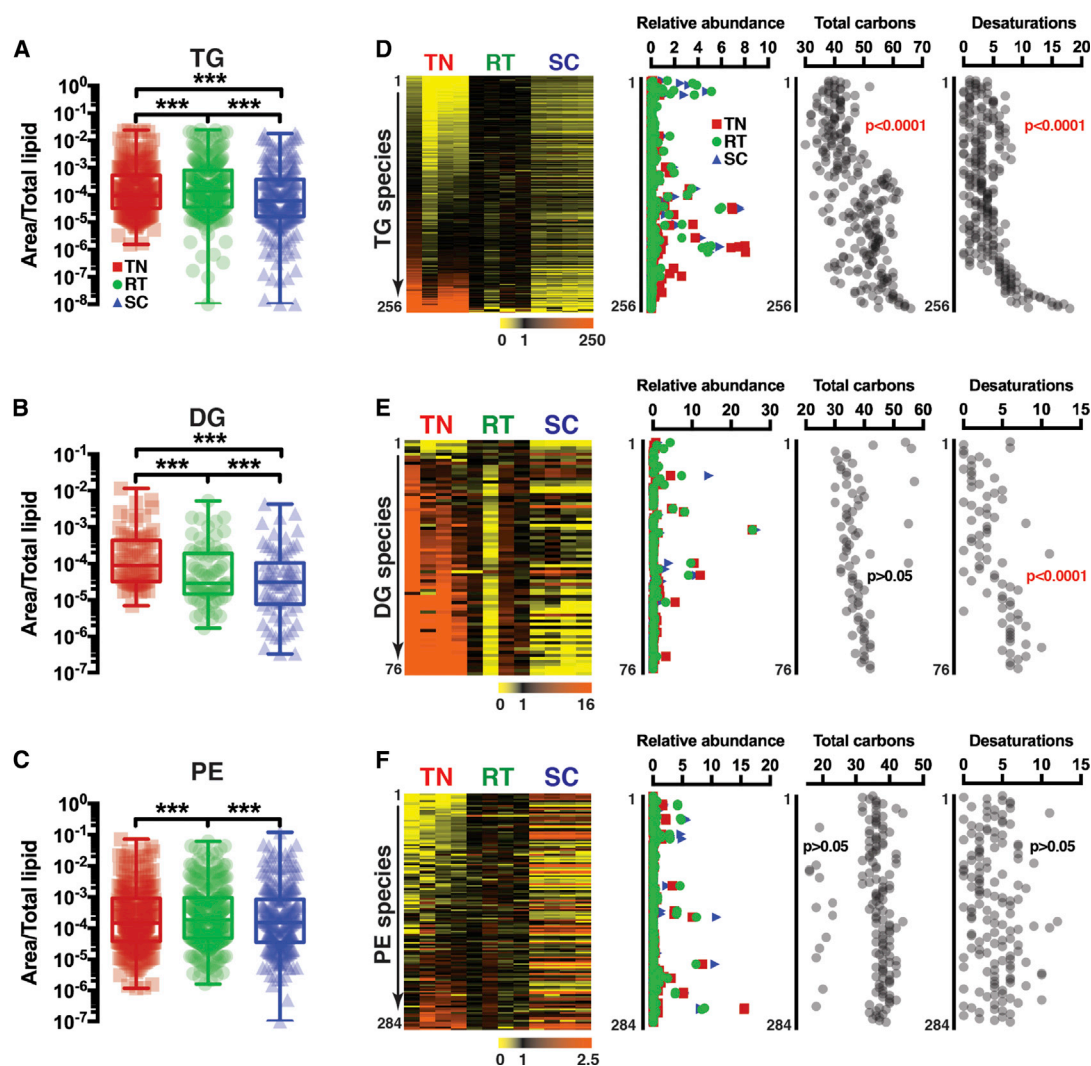
Figure 2. Environmental Temperature Remodels the BAT Lipid Landscape

(A–C) Abundance and distribution of TG (triacylglyceride), DG (diacylglyceride), and PE (phosphatidylethanolamines) species in iBAT of C57BL/6J mice at TN, RT, and SC housing conditions (n = 4). Each data point represents one species.

(D–F) Heatmaps of the TG, DG, and PE species in iBAT of C57BL/6J mice at TN, RT, and SC housing conditions sorted by the fold change between TN and RT conditions. For each heatmap, the associated graphs represent relative abundance, total carbons, and total desaturations in each species ordered according to the heatmap. Colors represent the fold change compared with the average of RT levels, set to 1. See scale in each heatmap.

***p < 0.001. See also Figure S2.

phosphorylation and Akt2-S474 phosphorylation (Figure S4F). Curiously, deleting *Akt2* increases AKT1-S473 phosphorylation; however, downstream Akt signaling indicated by Pras40-T246 and AS160-T642 phosphorylation is attenuated in both *Akt2* knockout models (Figure S4F). Thus, BAT requires AKT2 to maintain normal tissue mass in the cold.

To further investigate AKT2 function in BAT, 9-week-old control and *Akt2^Ucp1CreER* mice were acclimated to TN or RT for 4 weeks. AKT2 ablation is maintained at both temperatures (Figure 3E), and neither total body mass (Figure 3F) nor glucose and insulin tolerance (Figure 3G) differ between cohorts. *Akt2^Ucp1CreER* mice maintain their overall small BAT and normal WAT mass compared with controls at TN (Figure 3F), and histological analysis shows smaller lipid droplets in the *Akt2^Ucp1CreER*

brown adipocytes at both temperatures (Figures 3H and S4D). Thus, AKT2 is required for maintaining normal BAT lipid content.

Unbiased gene expression analysis on iBAT samples revealed little change in gene expression between controls and knockout mice at TN (Figure 3I), which is consistent with the low BAT AKT2 expression at TN. In contrast, we identified 753 genes differentially expressed at RT that partition into 339 increasing and 424 decreasing, respectively (Figure 3I). BAT AKT2 loss decreases expression of genes functioning in glycolysis, cholesterol and FA synthesis, amino acid metabolism, TCA cycle metabolism, glycogen metabolism, and the pentose phosphate pathway (Figure S4G), indicating that normally BAT utilizes AKT2 signaling to drive a significant fraction of its cold-stimulated metabolic program.
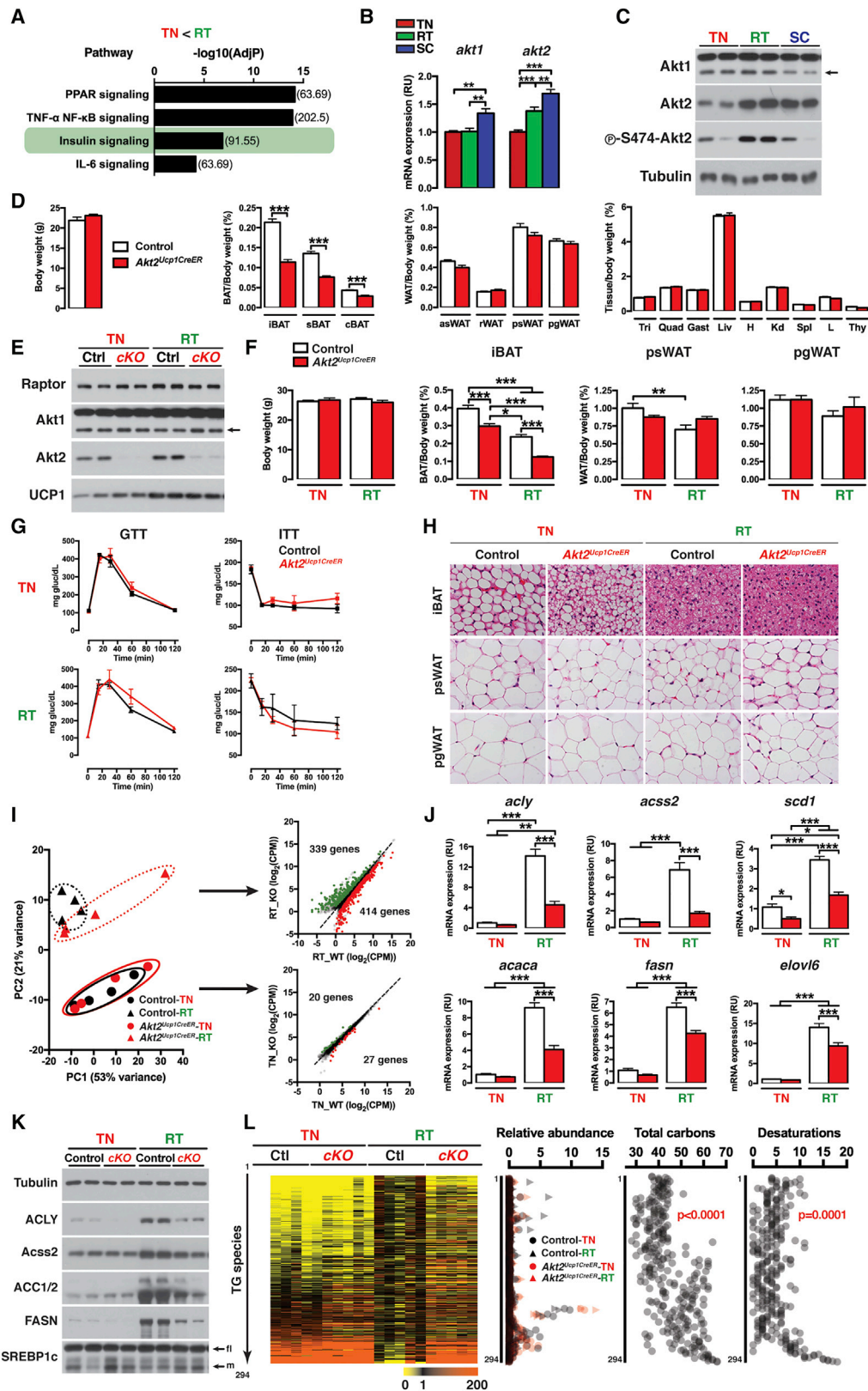
Figure 3. Mild Cold Induces AKT2 in BAT to Promote Lipid Storage and Lipid Remodeling

(A) BAT signaling pathways upregulated at RT compared with TN in C57BL/6J mice. AdjP, adjusted p value. Category ratio of enrichment (R, observed number of genes in the category versus expected) is shown in brackets.

Among the genes most significantly reduced by AKT2 loss in RT-adapted mice are *acly, acss2, acaca*, and *fasn* (Table S1, RNA-seq and lipidomics data related to Figure 3), which we confirmed by qPCR (Figure 3J) and western blot (Figure 3K), although notably ACSS2 protein levels are less impaired by AKT2 loss, suggesting that an AKT2-independent mechanism may also influence ACSS2 protein levels. AKT2 loss also reduces expression of *scd1* and *elovl6* (Figure 3J). Similar results were obtained with the constitutive BAT *Akt2* knockout at RT (Figure S4H). The global lipid profiles of TN-adapted control and *Akt2*^{Ucp1CreER} mice, like the gene expression signatures, are also similar (Figures 3L and S3B; Table S1, RNA-seq and lipidomics data related to Figure 3); however, there are significant differences at RT. For example, the TGs of RT-adapted *Akt2*^{Ucp1CreER} mice have shorter acyl side chains and more desaturations, similar to the TN profiles (Figure 3L). These data indicate that the cold-induced elevation of DNL genes and TG remodeling requires AKT2.

AKT2 Drives DNL Genes by Stimulating ChREBP Activity

Next, we sought to understand the mechanism by which AKT2 drives DNL gene expression. In mice living at RT, the gene coding SREBP1 (*Srebf1*), a transcription factor well-known to drive lipid metabolism downstream of insulin/AKT signaling in the liver (Leavens et al., 2009), is also highly expressed in all brown and white fat depots (Figure 4A). ChREBP, which senses intracellular glucose metabolites, and targets genes that overlap with SREBP1 (Jeong et al., 2011), is also emerging as a critical driver of hepatic lipid metabolism (Baraille et al., 2015; Denechaud et al., 2008) and white adipocyte DNL (Eissing et al., 2013; Herman et al., 2012; Tang et al., 2016). Using a tissue gene expression library, we observe little difference in *Srebf1* mRNA levels between BAT and WAT depots, while the full-length *ChREBP*α isoform is most highly expressed in the liver (Figure 4A). In contrast, the *ChREBP*β isoform, which is transcribed by ChREBPα from an alternative start site and encodes a truncated ChREBP protein with more potent transcriptional activity (Herman et al., 2012), is most highly expressed in BAT (Figure 4A). High BAT *ChREBP*β expression correlates with relatively high expression of *acly, acss2, acaca, fasn*, and *glut4* compared with other tissues. Expression of *acss1, acss2*, and *acss3* are also relatively high in BAT (Figure 4A). Thus, the genes encoding SREBP1, ChREBPβ, and major lipogenic genes are highly expressed in BAT.

To determine which lipogenic transcription factor might function downstream of AKT2, we analyzed the effects of environmental housing temperature on *srebf1* and *ChREBP*α expression levels. This did not reveal any differences in *sreb1f* expression across all three conditions, and there was a small but significant increase in *ChREBP*α expression with cold (Figure 4B). In contrast, relative to TN conditions, *ChREBP*β is induced by 12.7-fold at RT and 28.5-fold at SC (Figure 4B). SREBP1 is also activated by proteolytic processing, which releases a transcriptionally active N-terminal fragment (Wang et al., 2015); however, the abundance of the mature nuclear-SREBP1 fragment in BAT is unaffected by temperature (Figure 1I), suggesting that ChREBP is downstream of AKT2 under these conditions. Consistently, the elevation of *ChREBP*β by mild cold is attenuated in the BAT of *Akt2*^{Ucp1CreER} mice (Figure 4C), while *ChREBP*α and *srebf1* expression (Figure 4C) and SREBP1c processing (Figure 3K) are unaffected. These data favor a model in which ChREBPα induces ChREBPβ, to drive DNL gene expression downstream of AKT2.

AKT2 stimulates glucose uptake in adipocytes (Bae et al., 2003), and this could explain the decrease in *ChREBP*β expression because ChREBPα is reportedly activated by glucose metabolites (Filhoulaud et al., 2013). Indeed, glucose uptake is decreased in *Akt2*^{Ucp1CreER} BAT (Figure S5A), as are the levels of proposed ChREBPα activators, glucose-6-phosphate (G6P), and fructose-2,6-biphosphate (F2,6P), the latter inferred from a decrease in the F2,6P precursor, fructose-6-phosphate (Figure S5B). Consistent with insulin's positive role in FA uptake (Goldberg et al., 2009; Stahl et al., 2002), deleting *Akt2* also reduces BAT palmitate uptake (Figure S5A). Thus, a combination of reduced DNL and FA uptake may cause the paucity of lipid in *Akt2*^{Ucp1CreER} BAT.

To directly investigate the link between AKT signaling and ChREBP-driven DNL, we developed cultured inducible AKT knockout (AKTiKO) brown adipocytes that recapitulate the *Akt2*-deletion-induced attenuation of glucose uptake and *ChREBP*β expression (Figures S5C and S5D). *In vitro*, this requires deleting both *Akt1* and *Akt2*, because deleting *Akt2* alone has little effect on Akt signaling or lipogenic protein levels (Figure S5E). AKTiKO cells have reduced downstream AKT signaling (Figure 4D), ACLY, ACC, and FASN expression (Figure 4D), and lipogenic activity (Figure S5F). Similar results were obtained in primary adipocytes after inducing *Akt1/2* deletion (Figures S5G and S5H). AKTiKO cells do not show obvious signs

(B) qRT-PCR analysis (n = 8).

(C) Corresponding western blots. Arrow indicates the AKT1 band.

(D) Body mass and individual organ weights from *Akt2*^{Ucp1CreER} and *Akt2 floxed* littermate controls at 9 weeks old and 3 weeks post tamoxifen (n = 11–13).

(E) Corresponding western blots. Arrow indicates the AKT1 band.

(F) Total body and fat depot mass (n = 8 at TN; n = 7 at RT).

(G) Glucose and insulin tolerance tests (n = 5).

(H) Representative H&E images of the indicated fat depots.

(I) Left: RNA-seq-based principal component (PC) analysis on sampled from iBAT (n = 4). Right: correlation scatterplot for each condition indicating the number of significantly affected genes between *Akt2*^{Ucp1CreER} and littermates. CPM, counts per million.

(J) qRT-PCR analysis of iBAT samples (n = 8 at TN; n = 7 at RT).

(K) Corresponding western blots.

(L) Heatmaps of the TG species in the iBAT of *Akt2*^{Ucp1CreER} and littermate controls based on fold change between TN and RT conditions in controls (n = 5). Associated graphs indicate relative abundance, total carbons, and total desaturations in each species order according to the heatmap. Colors represent fold change compared with the average of Control-RT levels, set to 1. See scale in each heatmap.

Bar graphs or data points represent mean ± SEM. *$p < 0.05$, **$p < 0.01$, ***$p < 0.001$. See also Figure S3.
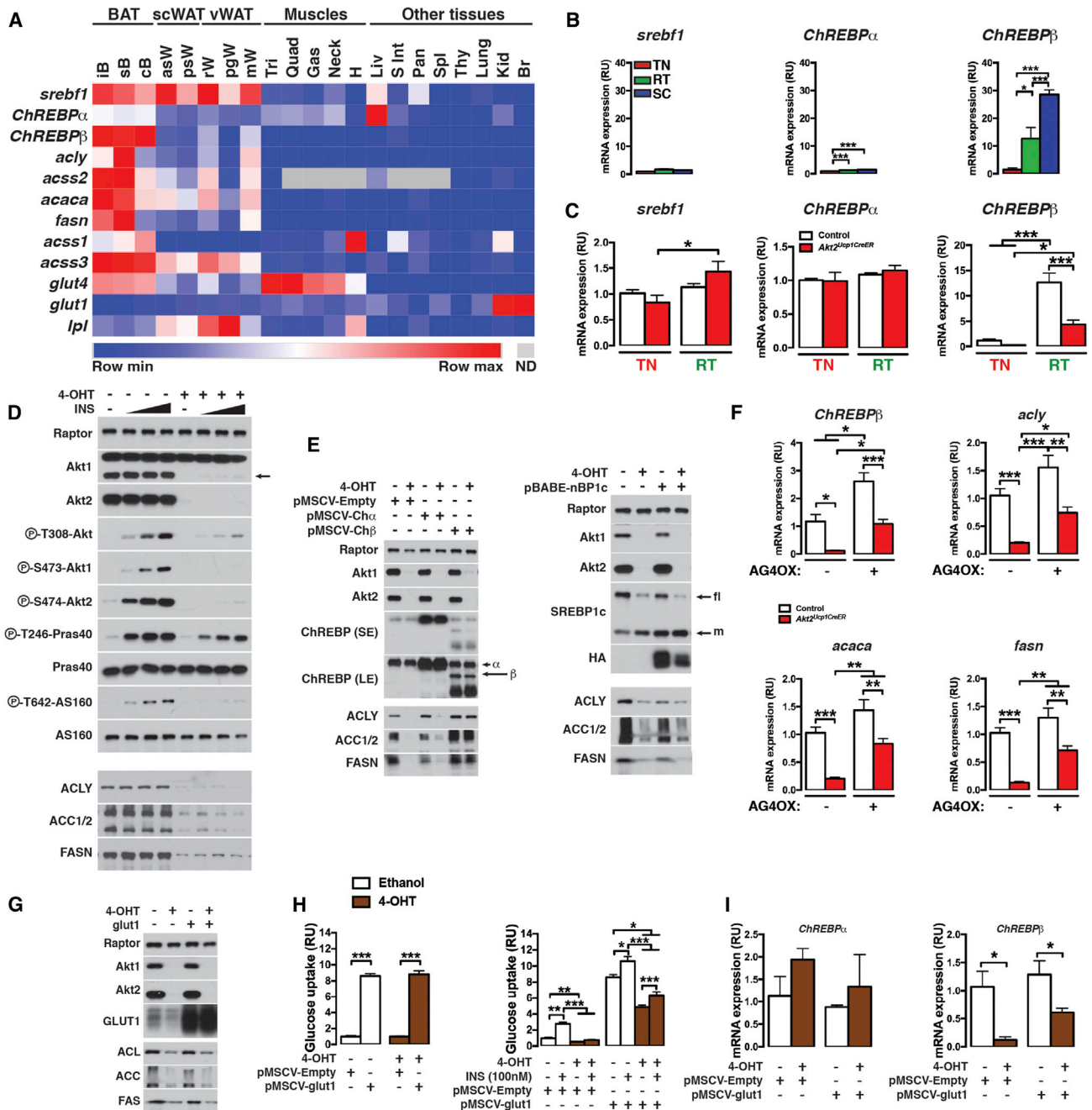
Figure 4. AKT2 Stimulates BAT DNL through ChREBP

(A) Gene expression levels of indicated genes in random fed C57BL/6J mice living at RT (n = 4). iB, interscapular BAT; sB, subscapular BAT; cB, cervical BAT; asW, anterior subcutaneous WAT; psW, posterior subcutaneous WAT; rW, retroperitoneal WAT; pgW, perigonadal WAT; mW, mesenteric WAT; Tri, triceps; Quad, quadriceps; Gas, gastrocnemius; H, heart; Liv, liver; S Int, small intestine; Pan, pancreas; Spl, spleen; Thy, thymus; Kid, kidneys; Br, brain; ND, not detected.

(B) qRT-PCR of iBAT samples from C57BL/6J mice adapted to TN, RT, and SC (n = 8).

(C) qRT-PCR of iBAT samples from *Akt2^Ucp1CreER^* and *Akt2 floxed* littermate controls (n = 8 at TN; n = 7 at RT).

(D) Western blot showing an insulin dose response (1–100 nM) in differentiated AKTiKO cells. Arrow indicates the AKT1 band.

(E) Western blot analysis of differentiated AKTiKO cells overexpressing plasmids containing ChREBP isoforms (pMSCV-Chα and pMSCV-Chβ) or the nuclear fragment of SREBP1c (pBABE-nBP1c).

(F) qRT-PCR analysis of iBAT from *Akt2^Ucp1CreER^* and controls with or without overexpressing human GLUT4 in adipose tissues (RT, n = 7).

(G) Western blot analysis of differentiated AKTiKO cells overexpressing recombinant GLUT1.

(H) Glucose uptake in differentiated AKTiKO cells overexpressing GLUT1. Each genotype is shown relative to cells expressing empty vector (n = 3).

(I) qRT-PCR analysis using differentiated AKTiKO cells overexpressing GLUT1 (n = 3).

Bar graphs represent mean ± SEM. *p < 0.05, **p < 0.01, ***p < 0.001. See also Figure S4.

of elevated lipolysis (Figures S5I and S5J). Cellular fractionation of AKTiKO cells in the presence of low or high glucose in the medium (5 versus 25 mM) showed a slight decrease in nuclear ChREBPα in AKTiKO cells (Figure S5K). However, only expressing ChREBPβ, and not vector, ChREBPα, or mature SREBP1, rescues ACLY, ACC, and FASN expression (Figure 4E) indicating expressing ChREBPβ is sufficient to rescue lipogenic gene expression in the absence of AKT.

Next, we asked if increasing glucose uptake is sufficient to rescue lipogenic gene expression in the absence of AKT2 signaling. We crossed $Akt2^{Ucp1CreER}$ mice with mice overexpressing human GLUT4 specifically in adipocytes (i.e., AG4Ox mice) because this increases adipose tissues basal glucose uptake by around 25-fold (Shepherd et al., 1993). Both the $AG4Ox$ and $Akt2^{Ucp1CreER}$;$AG4Ox$ mice express equally high levels of GLUT4 compared with their non-transgenic matched controls (Figure S5L); however, this did not rescue BAT mass or lipid levels (Figures S5M and S5N). Overexpressing GLUT4 did boost $ChREBPβ$ expression, but it remained markedly less compared with AG4Ox controls (Figure 4F, S5O), which was mirrored by $acly$, $acaca$, and $fasn$ (Figure 4F). One interpretation is that AKT2 may regulate an additional ChREBP-activating step. To test this in another way, we overexpressed the facilitated GLUT1 transporter in AKTiKO cells (Figure 4G). This increases basal glucose uptake in both control and AKTiKO cells by 8.6- and 8.8-fold, respectively, and to levels much higher than insulin-stimulated glucose uptake in empty vector control cells (Figure 4H), but has only a modest effect on $ChREBPβ$ expression (Figure 4I) and no effect on ACLY, ACC, or FASN levels (Figure 4G). Thus, glucose uptake alone may not be sufficient to fully stimulate ChREBP in the absence of AKT signaling.

BAT AKT2 Is Not Required to Maintain Euthermia, but Its Loss Enhances WAT Browning

The induction of AKT2 and DNL with cold led to the hypothesis that BAT AKT2-mediated DNL is required for optimal thermogenesis. To test this, we asked whether mice lacking BAT AKT2 can tolerate SC. $Ucp1$ mRNA and protein express at similar levels in the BAT of $Akt2^{Ucp1CreER}$ mice (Figures 5A and 3E), and BAT heat production shows no difference compared with controls (Figure S6A). Consistently, RT-adapted $Akt2^{Ucp1CreER}$ mice have normal body temperature and they do not become hypothermic when acutely challenged with SC (4°C) (Figure 5B); in fact, they tend to have a slightly warmer body temperature (Figures 5B and S6B). Thermogenic markers ($ucp1$, $elovl3$, and $pgc1α$) induce normally or slightly higher (Figure 5C). Food intake, plasma glucose, and weight loss was similar between groups (Figure S6C). Thus, $Akt2^{Ucp1CreER}$ mice are capable of maintaining euthermia in mild cold, and despite their BAT depots being smaller and lipid depleted, they appear to support basal thermogenesis.

Because thermogenesis is an adaptive response and shivering can significantly contribute to thermogenesis in an acute cold challenge (Cannon and Nedergaard, 2004, 2011), we next asked if $Akt2^{Ucp1CreER}$ can endure a prolonged (2-week) cold challenge. The $Akt2^{Ucp1CreER}$ mice maintain normal body weight, body temperature, and food consumption in prolonged cold despite having reduced BAT mass (Figures 5D–5H and S6D). However, psWAT mass increases in $Akt2^{Ucp1CreER}$ mice relative to controls

(Figure 5D), and this correlates with higher $Ucp1$ mRNA and protein induction and higher tyrosine hydroxylase levels (Figures 5I and 5K). During the challenge, AKT2 mRNA and protein remained ablated in BAT, while its levels were unvaried or elevated in psWAT and pgWAT, respectively (Figures 5I and 5J). This indicates a greater recruitment of brite/beige adipocytes, which was confirmed by histology (Figure 5H). Thus, while AKT2-driven DNL is not required for the thermogenic gene program, basal BAT activity, or for maintaining euthermia, mice that lack BAT AKT2 recruit more brite/beige adipocytes to cope with prolonged cold exposure.

A Diabetogenic Diet and AKT2 Loss Have Similar Effects on Adipocyte DNL

Decreased adipocyte DNL is linked to systemic insulin resistance and, although several mechanistic connections are proposed (Eissing et al., 2013; Herman et al., 2012; Tang et al., 2016), definitive link(s) remain unclear. We asked if a diabetogenic diet might impair DNL gene expression in BAT, similar to AKT2 loss, because one hypothesis is that diet-induced attenuation of AKT and/or DNL, among other mechanisms, could alter thermogenesis. Two weeks of high-fat diet (HFD), which causes modest insulin resistance (Tang et al., 2016), reduces $ChREBPβ$, $acly$, $acss2$, $acaca$, and $fasn$ gene expression in BAT to levels comparable with deleting $Akt2$, although there is an additional decrease by combining HFD and AKT2 loss (Figure 6A). Western blots mirror this for ACLY and FASN (Figure 6B). Interestingly, ACSS2 protein levels remain elevated in the BAT of $Akt2^{Ucp1CreER}$ mice on chow, despite its mRNA being reduced. HFD did, however, reduce ACSS2 mRNA and protein (Figures 6A and 6B) consistent with ACSS2 levels also having AKT2-independent regulation. Importantly, 2-week HFD attenuates AKT2-S474 phosphorylation in wild-type mice, while AKT1-S473 phosphorylation is unchanged (Figure 6B), indicating the negative effect of HFD on DNL corresponds with decreased AKT2 stimulation in wild-type mice. Note that AKT1-S473 phosphorylation increases when $Akt2$ is deleted, which may provide some compensatory activity (Figure S4F). Twelve weeks of HFD, however, decreases both AKT1-S473 and AKT2-S474 phosphorylation in wild-type mice (Figure S7A), consistent with prolonged HFD causing more severe insulin resistance. These data are consistent with diabetogenic diets impairing BAT DNL at least in part by dampening AKT2 signaling.

Two-week HFD also impairs DNL in WAT (Tang et al., 2016), questioning whether AKT2 might also regulate the ChREBPβ-DNL pathway in white adipocytes. To test this, we generated $Akt2^{AdipoqCre}$ mice. Indeed, mice lacking AKT2 in WAT have significantly reduced $ChREBPβ$ and DNL enzyme mRNA and protein expression with normal mature SREBP1c levels (Figures 6C and 6D), and this correlates with reduced tissue mass (Figures S7B and S7C) and adipocyte size (Figure S7D). Curiously, while the DNL pathway is also dramatically reduced in the BAT of $Akt2^{AdipoqCre}$ mice (Figure 6D), BAT mass is unaffected (Figure S7B) possibly reflecting increased lipid flux from WAT to non-WAT tissues, also suggested by the corresponding increase in liver mass. Regardless, these data argue that AKT2 also stimulates ChREBPβ-driven DNL in WAT and that diabetogenic diets might impinge upon the AKT2-ChREBPβ-DNL pathway to affect insulin sensitivity.
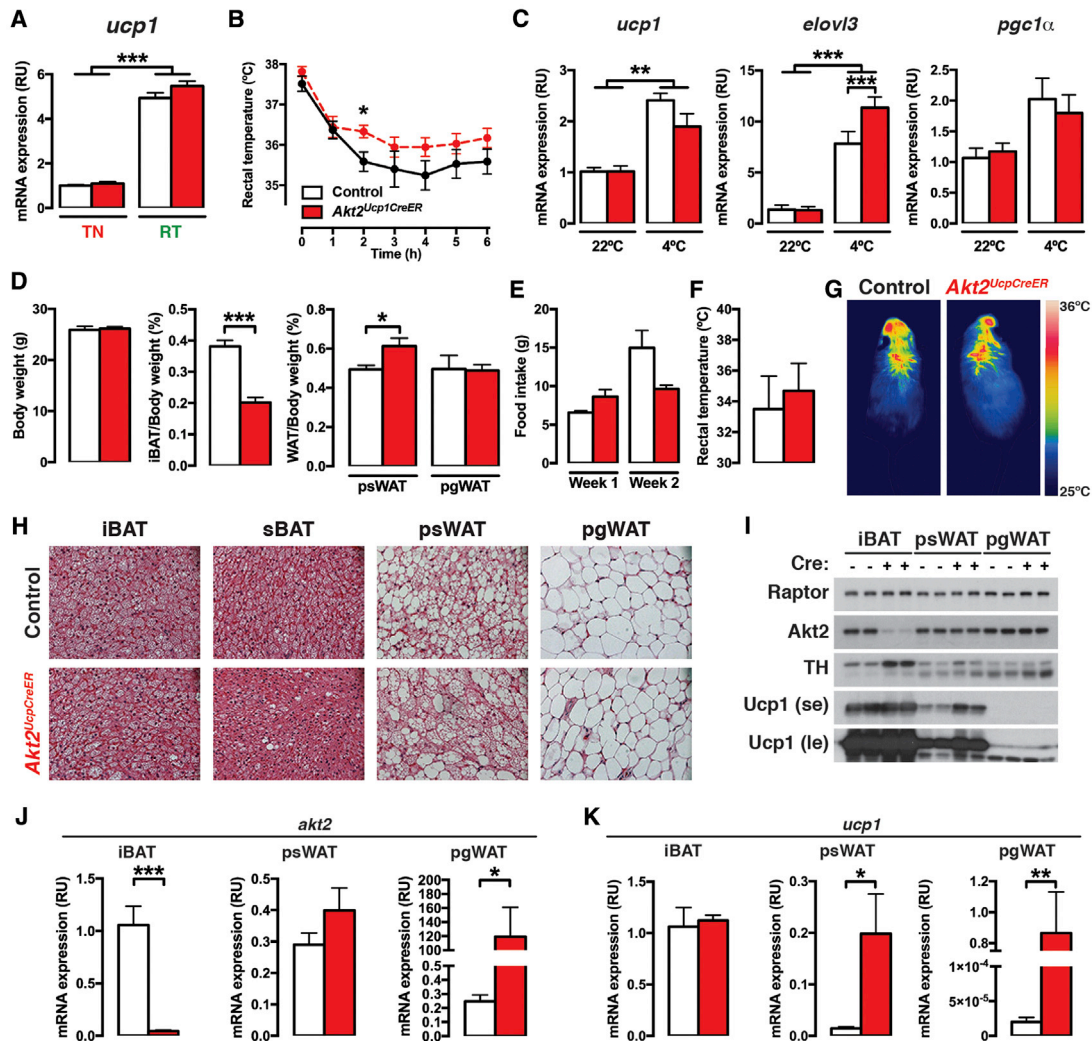
Figure 5. BAT AKT2 Is Not Required to Maintain Euthermia, but Its Loss Enhances WAT Browning

(A) qRT-PCR analysis of iBAT from *Akt2*[Ucp1CreER] and *Akt2 floxed* littermate controls (n = 8 at TN; n = 7 at RT).

(B) Rectal temperature in an acute cold challenge (4°C) starting from RT (n = 7).

(C) qRT-PCR analysis of iBAT after acute cold challenge (n = 7).

(D) Total body mass and fat depot weights after 2 weeks at 5°C (n = 6–7).

(E) Daily food intake per mouse during a 2-week adaptation to 5°C (n = 2 cages).

(F) Rectal temperature after 2 weeks at 5°C (n = 6–7).

(G) Thermal camera imaging after 2 weeks at 5°C.

(H) Representative H&E images after 2 weeks at 5°C.

(I) Western blot of iBAT, psWAT, and pgWAT lysates from *Akt2*[Ucp1CreER] and *Akt2 floxed* littermates after 2 weeks at 5°C.

(J) *Akt2* qRT-PCR analysis of fat tissues from *Akt2*[Ucp1CreER] and *Akt2 floxed* littermates after 2 weeks at 5°C (n = 6).

(K) Corresponding *ucp1* qRT-PCR analysis (n = 6).

Bar graphs represent mean ± SEM. *p < 0.05, **p < 0.01, ***p < 0.001. See also Figure S5.

ChREBPβ and *Ucp1* Expression Correlate in Human Brown Fat

Finally, we asked whether high *ChREBPβ* expression is a marker of active human brown adipocytes. Reflecting a life at thermoneutrality, it has been shown that brown fat in adult humans is heterogeneous in terms of multilocularity and UCP1 mRNA expression. High levels of UCP1 have been shown to correlate with the expression of the brown fat gene program transcriptional co-activators PGC-1α and PRDM16, and might together be assigned as "brown fat activity genes" (Jespersen et al., 2013). Thus, we compared the mRNA levels of *chrebpα*, *chrebpβ*, *srebp1c*, and *fasn* with *ucp1* in human BAT biopsies obtained from the supraclavicular region (Jespersen et al., 2013). We found no correlation between *srebp1c* or *chrebpα* with *ucp1* (Figures 7A–7D). However, *chrebpβ* levels positively correlate with *ucp1*, and its expression is 5-times higher in UCP1^{high} compared with UCP1^{low} samples (Figures 7E and 7F). Consistently, *fasn* expression also correlates with *ucp1* expression, and is 3-fold
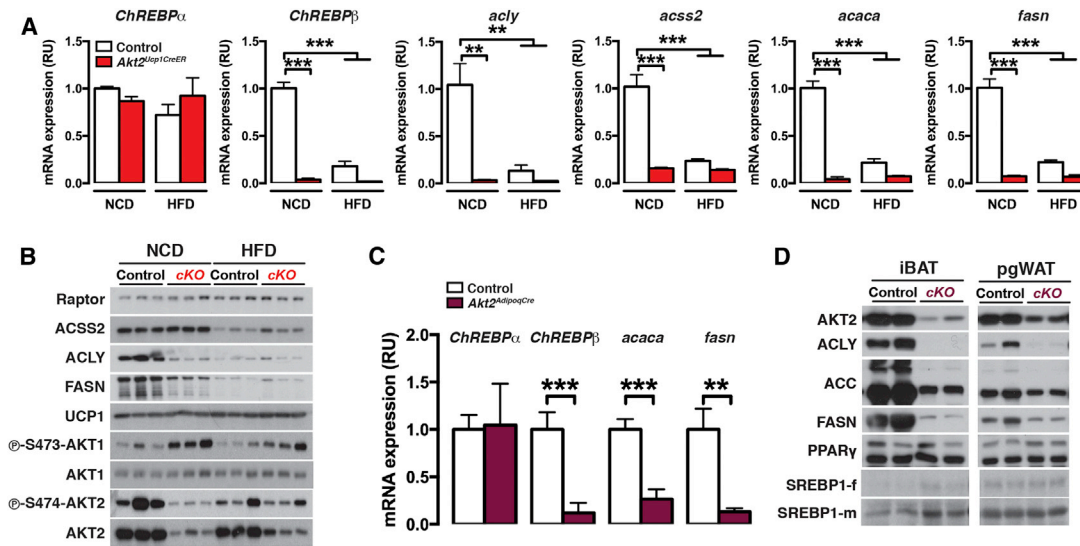
Figure 6. Short-Term High-Fat Diet Inhibits BAT DNL and the Phosphorylation of AKT2, Which also Drives ChREBP-Mediated DNL in WAT

(A) qRT-PCR analysis of iBAT from *Akt2^UcpCreER* and *Akt2 floxed* littermate controls at RT after 2 weeks of normal chow (NCD) or HFD feeding (n = 3).

(B) Corresponding western blot analysis.

(C) qRT-PCR analysis of posterior subcutaneous WAT from 8-week-old *Akt2^AdipoqCre* and *Akt2 floxed* littermate control mice living at RT (n = 8).

(D) Corresponding western blot for iBAT and pgWAT.

Bar graphs represent mean ± SEM. **p < 0.01, ***p < 0.001. See also Figures S6 and S7.

higher in UCP1^high compared with UCP1^low samples (Figures 7G and 7H). These data suggest that a similar role for ChREBP-driven DNL in BAT exists in humans.

DISCUSSION

DNL positively correlates with thermogenesis in BAT (McCormack and Denton, 1977; Mottillo et al., 2014; Shimazu and Takahashi, 1980; Townsend and Tseng, 2015; Trayhurn, 1979; Yu et al., 2002) and insulin sensitivity in WAT (Eissing et al., 2013; Herman et al., 2012; Tang et al., 2016), but its functional significance has been enigmatic. Here, we examined BAT gene expression in mice adapted to thermoneutrality, mild cold, and SC. Among the *most* upregulated genes by mild cold, a temperature range more physiologically relevant to humans, are genes controlling DNL. This was surprising given BAT's prominent catabolic role in absorbing and oxidizing lipids (Bartelt et al., 2011; Lee et al., 2015, 2016). The upregulation of DNL depends upon AKT2, which is also induced by mild cold. How mild cold induces AKT2 requires further investigation, but one possibility is that ChREBP regulates AKT2 through a feedforward mechanism as putative ChREBP binding activity has been reported in the *Akt2* promoter (Poungvarin et al., 2015). Importantly, the absence of BAT AKT2 results in more brite/beige adipocytes being recruited in the subcutaneous fat upon prolonged SC exposure indicating that the Akt2-ChREBP-DNL pathway is required for optimum BAT function. Finally, high UCP1 and DNL gene expression correlate in humans suggesting functional conservation.

Active brown fat is one of the most insulin-sensitive tissues (Cannon and Nedergaard, 2004), and thus cold may induce BAT AKT2 to ensure this. Mice lacking the insulin receptor in Myf5-derived brown adipocytes also have reduced lipogenic

gene expression in BAT and increased WAT browning (Lynes et al., 2015; Sanchez-Gurmaches and Guertin, 2014), favoring insulin as the key AKT2 agonist driving DNL in BAT. An alternative possibility is that β-adrenergic signaling stimulates AKT2. One study examining chronic β3-adrenergic stimulation found that treating mice for 7 days with CL316,243 increases DNL in BAT (Mottillo et al., 2014). An elegant model was proposed in which CL316,243-induced lipolysis releases FA metabolites that activate the PPARα and δ transcription factors to express lipogenic genes. Because these mice were mildly cold at the start of treatment, and thus already have high ChREBP activity, this could represent an additional mechanism to further boost DNL. Notably, CL316,243 also stimulates insulin secretion (Atef et al., 1996; de Souza et al., 1997; Yoshida et al., 1994). Additional signals such as thyroid hormones further help balancing FA synthesis and oxidation (Broeders et al., 2016; Weiner et al., 2016; Yeh et al., 1993). Understanding how multiple signaling and metabolic pathways intersect to promote BAT metabolism is critical to developing therapies targeting thermogenesis.

Fueling BAT Metabolism

Why is the AKT2-ChREBP-DNL pathway important for BAT function? It may provide additional fuel for thermogenesis, or help replenish lipid droplets. Alternatively, certain *de novo* synthesized lipids could have intracellular signaling or paracrine/endocrine "batokine"-like functions (Cao et al., 2008; Yore et al., 2014). However, another underappreciated feature of increased DNL is the corresponding increase in metabolic intermediates that have signaling functions, such as acetyl-CoA and malonyl-CoA, the former being the acetyl donor for protein lysine acetylation (Pietrocola et al., 2015). Increased post-translational
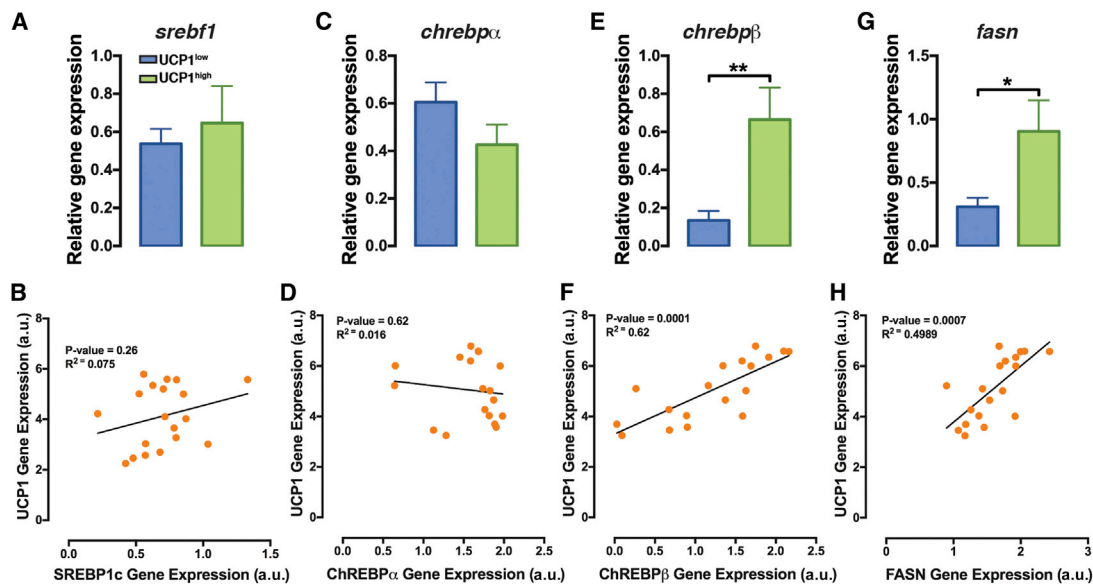
Figure 7. *Chrebpβ* and *Fasn* Expression Positively Correlate with *Ucp1* in Human Brown Adipocytes
(A, C, E, and G) Gene expression in human BAT with low (UCP1^{low}) or high (UCP1^{high}) levels of activation (n = 9–10).
(B, D, F, and H) Correlation plots between indicated genes and ucp1 levels in human BAT. a.u., arbitrary units.
Bar graphs represent mean ± SEM. *$p < 0.05$, **$p < 0.01$.

modifications, including epigenetic signals driven by high glucose and/or acetate metabolism to bioactive intermediate metabolites, could have key roles in maintaining lipid homeostasis in adipose tissues.

A role in BAT for cytoplasmic acetyl-CoA generated by ACSS2 is not well appreciated. Acetate is an important fuel in certain cancer cells (Comerford et al., 2014; Mashimo et al., 2014) and in white adipocytes lacking ACLY (Zhao et al., 2016). Acetate is obtained within the cell from the deacetylation of proteins (e.g., histones), from acetyl-CoA hydrolases, or exogenously from circulation. Acetate levels in mouse and human serum ranges from 50 to 600 μM (Hosios and Vander Heiden, 2014) and is obtained from the liver, from dietary nutrients (largely through the gut microbiota), and from ethanol (Hosios and Vander Heiden, 2014). Elucidating the sources and fates of acetyl-CoA in BAT metabolism is an important future direction.

The paradox that BAT simultaneously upregulates catabolic and anabolic lipid metabolism runs counterintuitive to classic models of substrate competition, such as the Randle cycle, in which FA oxidation inhibits glucose metabolism. Moreover, malonyl-CoA generated during lipid synthesis inhibits FA oxidation by inhibiting carnitine palmitoyltransferase 1 (CPT1) (Hue and Taegtmeyer, 2009). This normally balances FA synthesis oxidation; however, BAT appears to override these checkpoints to meet its metabolic demands. We noted in our gene expression data that peroxisome biogenesis genes increase, while *Cpt1a* and *Cpt1c* levels decrease, at RT compared with TN (Figure S2A). One possibility is that increased peroxisomal oxidation may reduce VLCFAs and LCFAs to medium-chain FAs of 12 carbons or fewer, which enter mitochondria independently of CPT1 (McDonnell et al., 2016; McGarry and Foster, 1971). Increased peroxisomal oxidation might also reduce pressure on the carnitine shuttle, which was also recently

shown to be required for thermogenesis (Lee et al., 2015, 2016). Peroxisomal-generated acetyl-CoA could also be used for lipid synthesis in a futile cycle. Peroxisomal activity in BAT is a process deserving more attention.

Regulation of DNL by AKT2-ChREBP

Two-week HFD reduces basal AKT2-S474 phosphorylation and DNL pathway enzyme expression in wild-type mice similar to deleting *Akt2* in chow fed mice. AKT2-S474 phosphorylation is stimulated by mammalian target of rapamycin complex 2 (mTORC2) (Lee et al., 2017; Sarbassov et al., 2005) and similar to deleting *Akt2,* deleting *Rictor* (an essential mTORC2 subunit) in BAT or WAT dramatically reduces DNL (Hung et al., 2014; Tang et al., 2016). Interestingly however, *Rictor* loss in adipocytes does not impair AKT signaling to many of its classic substrates. It is possible that an unidentified mTORC2-AKT pathway regulates DNL, or that AKT2 and mTORC2 converge on DNL through different mechanisms. Nevertheless, DNL in adipocytes is negatively affected by HFD, which could impinge upon the mTORC2 and/or AKT2 pathway. Interestingly, only a few days of HFD feeding can inhibit glucose uptake into (white) adipose tissue and cause hepatic insulin resistance without inhibiting AKT phosphorylation (Turner et al., 2013). One possibility is that short-term HFD specifically targets the AKT-DNL pathway. Alternatively, AKT-independent attenuation of glucose uptake could be an acute effect of HFD compounded later by reduced AKT2 activity. The latter hypothesis is consistent with our data showing that ChREBP may be regulated by an additional AKT-independent mechanism. AKT signaling is also implicated in lipolysis although the mechanism is debated (Choi et al., 2010; DiPilato et al., 2015; Nielsen et al., 2014), and while not pursued further here it remains possible that anti-lipolytic AKT2 functions are coordinated with its lipogenic functions to control

BAT metabolism. Understanding how mTORC2, AKT2, and dietary fats converge on lipid metabolism in adipocytes requires a much deeper understanding than we have at present about how and where these pathways interconnect in cells.

In conclusion, we have identified a novel lipogenic axis in brown fat during acclimation to mild cold. Our mechanistic findings are supported by human data, and future studies are thus warranted to investigate the clinical importance of this axis.

STAR★METHODS

Detailed methods are provided in the online version of this paper and include the following:

- KEY RESOURCES TABLE
- CONTACT FOR REAGENT AND RESOURCE SHARING
- EXPERIMENTAL MODEL AND SUBJECT DETAILS
  - Mice and Mice Housing
  - Cell Culture
  - Human BAT
- METHOD DETAILS
  - Tissue Dissection
  - Tamoxifen Treatment
  - Acute/Prolong Cold Challenge
  - Fasting/Refeeding
  - High Fat Diet Feeding
  - Temperature Measurements
  - Glucose and Insulin Tolerance Tests
  - In Vivo Glucose and FA Uptake
  - Tissue Histology
  - Metabolite Profiling
  - Gene Expression and Western Blot Analysis
  - Whole Mount Confocal Microscopy
  - Gene Expression Profile
  - In Vivo Lipogenesis Assay
  - In Vitro Lipogenesis Assay
  - Human Brown Fat Analysis
- QUANTIFICATION AND STATISTICAL ANALYSIS
- DATA AND SOFTWARE AVAILABILITY

SUPPLEMENTAL INFORMATION

Supplemental Information includes seven figures and four tables and can be found with this article online at https://doi.org/10.1016/j.cmet.2017.10.008.

AUTHOR CONTRIBUTIONS

M.W. and C.M.M. analyzed D2O incorporation. N.Z.J., S.N., and C.S. obtained and analyzed human brown fat. C.M.C. made AKTiKO cells. H.L. assisted with animal husbandry and genotyping. S.G. and Y.J.K.E. performed the bioinformatics analysis of the RNA-seq data. C.W. generated *Ucp1-Cre^ER* mice and valuable discussions. Y.T. generated and analyzed *Akt2^AdipoqCre* mice and helped with HFD experiments. J.S.G. and D.A.G. conceptualized the study, interpreted data, and wrote the manuscript. J.S.G. performed most of the experiments. All authors approved of the manuscript.

REFERENCES

Atef, N., Lafontan, M., Double, A., Helary, C., Ktorza, A., and Penicaud, L. (1996). A specific beta 3-adrenoceptor agonist induces increased pancreatic islet blood flow and insulin secretion in rats. Eur. J. Pharmacol. *298*, 287–292.

Bae, S.S., Cho, H., Mu, J., and Birnbaum, M.J. (2003). Isoform-specific regulation of insulin-dependent glucose uptake by Akt/protein kinase B. J. Biol. Chem. *278*, 49530–49536.

Baraille, F., Planchais, J., Dentin, R., Guilmeau, S., and Postic, C. (2015). Integration of ChREBP-mediated glucose sensing into whole body metabolism. Physiology (Bethesda) *30*, 428–437.

Bartelt, A., Bruns, O.T., Reimer, R., Hohenberg, H., Ittrich, H., Peldschus, K., Kaul, M.G., Tromsdorf, U.I., Weller, H., Waurisch, C., et al. (2011). Brown adipose tissue activity controls triglyceride clearance. Nat. Med. *17*, 200–205.

Broeders, E.P., Vijgen, G.H., Havekes, B., Bouvy, N.D., Mottaghy, F.M., Kars, M., Schaper, N.C., Schrauwen, P., Brans, B., and van Marken Lichtenbelt, W.D. (2016). Thyroid hormone activates brown adipose tissue and increases non-shivering thermogenesis – a cohort study in a group of thyroid carcinoma patients. PLoS One *11*, e0145049.

Cannon, B., and Nedergaard, J. (2004). Brown adipose tissue: function and physiological significance. Physiol. Rev. *84*, 277–359.

Cannon, B., and Nedergaard, J. (2011). Nonshivering thermogenesis and its adequate measurement in metabolic studies. J. Exp. Biol. *214*, 242–253.

Cao, H., Gerhold, K., Mayers, J.R., Wiest, M.M., Watkins, S.M., and Hotamisligil, G.S. (2008). Identification of a lipokine, a lipid hormone linking adipose tissue to systemic metabolism. Cell *134*, 933–944.

Choi, S.M., Tucker, D.F., Gross, D.N., Easton, R.M., DiPilato, L.M., Dean, A.S., Monks, B.R., and Birnbaum, M.J. (2010). Insulin regulates adipocyte lipolysis via an Akt-independent signaling pathway. Mol. Cell Biol. *30*, 5009–5020.

Comerford, S.A., Huang, Z., Du, X., Wang, Y., Cai, L., Witkiewicz, A.K., Walters, H., Tantawy, M.N., Fu, A., Manning, H.C., et al. (2014). Acetate dependence of tumors. Cell *159*, 1591–1602.

Cypess, A.M., Lehman, S., Williams, G., Tal, I., Rodman, D., Goldfine, A.B., Kuo, F.C., Palmer, E.L., Tseng, Y.H., Doria, A., et al. (2009). Identification and importance of brown adipose tissue in adult humans. N. Engl. J. Med. *360*, 1509–1517.

de Souza, C.J., Hirshman, M.F., and Horton, E.S. (1997). CL-316,243, a beta3-specific adrenoceptor agonist, enhances insulin-stimulated glucose disposal in nonobese rats. Diabetes *46*, 1257–1263.

Denechaud, P.D., Bossard, P., Lobaccaro, J.M., Millatt, L., Staels, B., Girard, J., and Postic, C. (2008). ChREBP, but not LXRs, is required for the induction of glucose-regulated genes in mouse liver. J. Clin. Invest. *118*, 956–964.

DiPilato, L.M., Ahmad, F., Harms, M., Seale, P., Manganiello, V., and Birnbaum, M.J. (2015). The role of PDE3B phosphorylation in the inhibition of lipolysis by insulin. Mol. Cell Biol. *35*, 2752–2760.

Dobin, A., Davis, C.A., Schlesinger, F., Drenkow, J., Zaleski, C., Jha, S., Batut, P., Chaisson, M., and Gingeras, T.R. (2013). STAR: ultrafast universal RNA-seq aligner. Bioinformatics 29, 15–21.

Eissing, L., Scherer, T., Todter, K., Knippschild, U., Greve, J.W., Buurman, W.A., Pinnschmidt, H.O., Rensen, S.S., Wolf, A.M., Bartelt, A., et al. (2013). De novo lipogenesis in human fat and liver is linked to ChREBP-beta and metabolic health. Nat. Commun. 4, 1528.

Fedorenko, A., Lishko, P.V., and Kirichok, Y. (2012). Mechanism of fatty-acid-dependent UCP1 uncoupling in brown fat mitochondria. Cell 151, 400–413.

Fernandez, C.A., Des Rosiers, C., Previs, S.F., David, F., and Brunengraber, H. (1996). Correction of 13C mass isotopomer distributions for natural stable isotope abundance. J. Mass Spectrom. 31, 255–262.

Filhoulaud, G., Guilmeau, S., Dentin, R., Girard, J., and Postic, C. (2013). Novel insights into ChREBP regulation and function. Trends Endocrinol. Metab. 24, 257–268.

Goldberg, I.J., Eckel, R.H., and Abumrad, N.A. (2009). Regulation of fatty acid uptake into tissues: lipoprotein lipase- and CD36-mediated pathways. J. Lipid Res. 50 (Suppl), S86–S90.

Guan, H.P., Li, Y., Jensen, M.V., Newgard, C.B., Steppan, C.M., and Lazar, M.A. (2002). A futile metabolic cycle activated in adipocytes by antidiabetic agents. Nat. Med. 8, 1122–1128.

Hall, A.M., Kou, K., Chen, Z., Pietka, T.A., Kumar, M., Korenblat, K.M., Lee, K., Ahn, K., Fabbrini, E., Klein, S., et al. (2012). Evidence for regulated monoacylglycerol acyltransferase expression and activity in human liver. J. Lipid Res. 53, 990–999.

Hanssen, M.J., Hoeks, J., Brans, B., van der Lans, A.A., Schaart, G., van den Driessche, J.J., Jorgensen, J.A., Boekschoten, M.V., Hesselink, M.K., Havekes, B., et al. (2015). Short-term cold acclimation improves insulin sensitivity in patients with type 2 diabetes mellitus. Nat. Med. 21, 863–865.

Harms, M., and Seale, P. (2013). Brown and beige fat: development, function and therapeutic potential. Nat. Med. 19, 1252–1263.

Herman, M.A., Peroni, O.D., Villoria, J., Schon, M.R., Abumrad, N.A., Bluher, M., Klein, S., and Kahn, B.B. (2012). A novel ChREBP isoform in adipose tissue regulates systemic glucose metabolism. Nature 484, 333–338.

Hosios, A.M., and Vander Heiden, M.G. (2014). Acetate metabolism in cancer cells. Cancer Metab. 2, 27.

Hue, L., and Taegtmeyer, H. (2009). The Randle cycle revisited: a new head for an old hat. Am. J. Physiol. Endocrinol. Metab. 297, E578–E591.

Hung, C.M., Calejman, C.M., Sanchez-Gurmaches, J., Li, H., Clish, C.B., Hettmer, S., Wagers, A.J., and Guertin, D.A. (2014). Rictor/mTORC2 loss in the Myf5 lineage reprograms brown fat metabolism and protects mice against obesity and metabolic disease. Cell Rep. 8, 256–271.

Jeong, Y.S., Kim, D., Lee, Y.S., Kim, H.J., Han, J.Y., Im, S.S., Chong, H.K., Kwon, J.K., Cho, Y.H., Kim, W.K., et al. (2011). Integrated expression profiling and genome-wide analysis of ChREBP targets reveals the dual role for ChREBP in glucose-regulated gene expression. PLoS One 6, e22544.

Jespersen, N.Z., Larsen, T.J., Peijs, L., Daugaard, S., Homoe, P., Loft, A., de Jong, J., Mathur, N., Cannon, B., Nedergaard, J., et al. (2013). A classical brown adipose tissue mRNA signature partly overlaps with brite in the supraclavicular region of adult humans. Cell Metab. 17, 798–805.

Kitamura, T., Kitamura, Y., Kuroda, S., Hino, Y., Ando, M., Kotani, K., Konishi, H., Matsuzaki, H., Kikkawa, U., Ogawa, W., et al. (1999). Insulin-induced phosphorylation and activation of cyclic nucleotide phosphodiesterase 3B by the serine-threonine kinase Akt. Mol. Cell. Biol. 19, 6286–6296.

Labbe, S.M., Caron, A., Bakan, I., Laplante, M., Carpentier, A.C., Lecomte, R., and Richard, D. (2015). In vivo measurement of energy substrate contribution to cold-induced brown adipose tissue thermogenesis. FASEB J. 29, 2046–2058.

Labbe, S.M., Caron, A., Chechi, K., Laplante, M., Lecomte, R., and Richard, D. (2016). Metabolic activity of brown, "beige," and white adipose tissues in response to chronic adrenergic stimulation in male mice. Am. J. Physiol. Endocrinol. Metab. 311, E260–E268.

Leavens, K.F., Easton, R.M., Shulman, G.I., Previs, S.F., and Birnbaum, M.J. (2009). Akt2 is required for hepatic lipid accumulation in models of insulin resistance. Cell Metab. 10, 405–418.

Lee, J., Choi, J., Aja, S., Scafidi, S., and Wolfgang, M.J. (2016). Loss of adipose fatty acid oxidation does not potentiate obesity at thermoneutrality. Cell Rep. 14, 1308–1316.

Lee, J., Ellis, J.M., and Wolfgang, M.J. (2015). Adipose fatty acid oxidation is required for thermogenesis and potentiates oxidative stress-induced inflammation. Cell Rep. 10, 266–279.

Lee, P.L., Jung, S.M., and Guertin, D.A. (2017). The complex roles of mechanistic target of rapamycin in adipocytes and beyond. Trends Endocrinol. Metab. 28, 319–339.

Lee, W.N., Bassilian, S., Ajie, H.O., Schoeller, D.A., Edmond, J., Bergner, E.A., and Byerley, L.O. (1994). In vivo measurement of fatty acids and cholesterol synthesis using D2O and mass isotopomer analysis. Am. J. Physiol. 266, E699–E708.

Lynes, M.D., Schulz, T.J., Pan, A.J., and Tseng, Y.H. (2015). Disruption of insulin signaling in Myf5-expressing progenitors leads to marked paucity of brown fat but normal muscle development. Endocrinology 156, 1637–1647.

Mashimo, T., Pichumani, K., Vemireddy, V., Hatanpaa, K.J., Singh, D.K., Sirasanagandla, S., Nannepaga, S., Piccirillo, S.G., Kovacs, Z., Foong, C., et al. (2014). Acetate is a bioenergetic substrate for human glioblastoma and brain metastases. Cell 159, 1603–1614.

McCabe, B.J., Bederman, I.R., Croniger, C., Millward, C., Norment, C., and Previs, S.F. (2006). Reproducibility of gas chromatography-mass spectrometry measurements of 2H labeling of water: application for measuring body composition in mice. Anal. Biochem. 350, 171–176.

McCormack, J.G., and Denton, R.M. (1977). Evidence that fatty acid synthesis in the interscapular brown adipose tissue of cold-adapted rats is increased in vivo by insulin by mechanisms involving parallel activation of pyruvate dehydrogenase and acetyl-coenzyme A carboxylase. Biochem. J. 166, 627–630.

McDonnell, E., Crown, S.B., Fox, D.B., Kitir, B., Ilkayeva, O.R., Olsen, C.A., Grimsrud, P.A., and Hirschey, M.D. (2016). Lipids reprogram metabolism to become a major carbon source for histone acetylation. Cell Rep. 17, 1463–1472.

McGarry, J.D., and Foster, D.W. (1971). The regulation of ketogenesis from octanoic acid. The role of the tricarboxylic acid cycle and fatty acid synthesis. J. Biol. Chem. 246, 1149–1159.

Mottillo, E.P., Balasubramanian, P., Lee, Y.H., Weng, C., Kershaw, E.E., and Granneman, J.G. (2014). Coupling of lipolysis and de novo lipogenesis in brown, beige, and white adipose tissues during chronic beta3-adrenergic receptor activation. J. Lipid Res. 55, 2276–2286.

Nedergaard, J., Bengtsson, T., and Cannon, B. (2007). Unexpected evidence for active brown adipose tissue in adult humans. Am. J. Physiol. Endocrinol. Metab. 293, E444–E452.

Nielsen, T.S., Jessen, N., Jorgensen, J.O., Moller, N., and Lund, S. (2014). Dissecting adipose tissue lipolysis: molecular regulation and implications for metabolic disease. J. Mol. Endocrinol. 52, R199–R222.

Ouellet, V., Labbe, S.M., Blondin, D.P., Phoenix, S., Guerin, B., Haman, F., Turcotte, E.E., Richard, D., and Carpentier, A.C. (2012). Brown adipose tissue oxidative metabolism contributes to energy expenditure during acute cold exposure in humans. J. Clin. Invest. 122, 545–552.

Pietrocola, F., Galluzzi, L., Bravo-San Pedro, J.M., Madeo, F., and Kroemer, G. (2015). Acetyl coenzyme a: a central metabolite and second messenger. Cell Metab. 21, 805–821.

Poungvarin, N., Chang, B., Imamura, M., Chen, J., Moolsuwan, K., Sae-Lee, C., Li, W., and Chan, L. (2015). Genome-wide analysis of ChREBP binding sites on male mouse liver and white adipose chromatin. Endocrinology 156, 1982–1994.

Purich, D.L., Fromm, H.J., and Rudolph, F.B. (1973). The hexokinases: kinetic, physical, and regulatory properties. Adv. Enzymol. Relat. Areas Mol. Biol. 39, 249–326.

Rau, A., Gallopin, M., Celeux, G., and Jaffrezic, F. (2013). Data-based filtering for replicated high-throughput transcriptome sequencing experiments. Bioinformatics 29, 2146–2152.

Robinson, M.D., McCarthy, D.J., and Smyth, G.K. (2010). edgeR: a Bioconductor package for differential expression analysis of digital gene expression data. Bioinformatics 26, 139–140.

Rosenwald, M., Perdikari, A., Rulicke, T., and Wolfrum, C. (2013). Bi-directional interconversion of brite and white adipocytes. Nat. Cell Biol. 15, 659–667.

Saito, M., Okamatsu-Ogura, Y., Matsushita, M., Watanabe, K., Yoneshiro, T., Nio-Kobayashi, J., Iwanaga, T., Miyagawa, M., Kameya, T., Nakada, K., et al. (2009). High incidence of metabolically active brown adipose tissue in healthy adult humans: effects of cold exposure and adiposity. Diabetes 58, 1526–1531.

Sanchez-Gurmaches, J., and Guertin, D.A. (2014). Adipocytes arise from multiple lineages that are heterogeneously and dynamically distributed. Nat. Commun. 5, 4099.

Sanchez-Gurmaches, J., Hung, C.M., and Guertin, D.A. (2016). Emerging complexities in adipocyte origins and identity. Trends Cell Biol. 26, 313–326.

Sarbassov, D.D., Guertin, D.A., Ali, S.M., and Sabatini, D.M. (2005). Phosphorylation and regulation of Akt/PKB by the rictor-mTOR complex. Science 307, 1098–1101.

Shepherd, P.R., Gnudi, L., Tozzo, E., Yang, H., Leach, F., and Kahn, B.B. (1993). Adipose cell hyperplasia and enhanced glucose disposal in transgenic mice overexpressing GLUT4 selectively in adipose tissue. J. Biol. Chem. 268, 22243–22246.

Shimazu, T., and Takahashi, A. (1980). Stimulation of hypothalamic nuclei has differential effects on lipid synthesis in brown and white adipose tissue. Nature 284, 62–63.

Shinoda, K., Luijten, I.H., Hasegawa, Y., Hong, H., Sonne, S.B., Kim, M., Xue, R., Chondronikola, M., Cypess, A.M., Tseng, Y.H., et al. (2015). Genetic and functional characterization of clonally derived adult human brown adipocytes. Nat. Med. 21, 389–394.

Stahl, A., Evans, J.G., Pattel, S., Hirsch, D., and Lodish, H.F. (2002). Insulin causes fatty acid transport protein translocation and enhanced fatty acid uptake in adipocytes. Dev. Cell 2, 477–488.

Steinberg, D., Vaughan, M., Margolis, S., Price Wttao, H., and Pittman, R. (1961). Studies of triglyceride biosynthesis in homogenates of adipose tissue. J. Biol. Chem. 236, 1631–1637.

Tang, Y., Wallace, M., Sanchez-Gurmaches, J., Hsiao, W.Y., Li, H., Lee, P.L., Vernia, S., Metallo, C.M., and Guertin, D.A. (2016). Adipose tissue mTORC2 regulates ChREBP-driven de novo lipogenesis and hepatic glucose metabolism. Nat. Commun. 7, 11365.

Townsend, K.L., and Tseng, Y.H. (2015). Of mice and men: novel insights regarding constitutive and recruitable brown adipocytes. Int. J. Obes. Suppl. 5, S15–S20.

Townsend, M.K., Clish, C.B., Kraft, P., Wu, C., Souza, A.L., Deik, A.A., Tworoger, S.S., and Wolpin, B.M. (2013). Reproducibility of metabolomic profiles among men and women in 2 large cohort studies. Clin. Chem. 59, 1657–1667.

Trayhurn, P. (1979). Fatty acid synthesis in vivo in brown adipose tissue, liver and white adipose tissue of the cold-acclimated rat. FEBS Lett. 104, 13–16.

Turner, N., Kowalski, G.M., Leslie, S.J., Risis, S., Yang, C., Lee-Young, R.S., Babb, J.R., Meikle, P.J., Lancaster, G.I., Henstridge, D.C., et al. (2013). Distinct patterns of tissue-specific lipid accumulation during the induction of insulin resistance in mice by high-fat feeding. Diabetologia 56, 1638–1648.

van Marken Lichtenbelt, W.D., Vanhommerig, J.W., Smulders, N.M., Drossaerts, J.M.A.F.L., Kemerink, G.J., Bouvy, N.D., Schrauwen, P., and Teule, G.J.J. (2009). Cold-activated brown adipose tissue in healthy men. N. Engl. J. Med. 360, 1500–1508.

Virtanen, K.A., Lidell, M.E., Orava, J., Heglind, M., Westergren, R., Niemi, T., Taittonen, M., Laine, J., Savisto, N.-J., Enerback, S., et al. (2009). Brief report: functional brown adipose tissue in healthy adults. N. Engl. J. Med. 360, 1518–1525.

Wan, M., Easton, R.M., Gleason, C.E., Monks, B.R., Ueki, K., Kahn, C.R., and Birnbaum, M.J. (2012). Loss of Akt1 in mice increases energy expenditure and protects against diet-induced obesity. Mol. Cell. Biol. 32, 96–106.

Wan, M., Leavens, K.F., Saleh, D., Easton, R.M., Guertin, D.A., Peterson, T.R., Kaestner, K.H., Sabatini, D.M., and Birnbaum, M.J. (2011). Postprandial hepatic lipid metabolism requires signaling through Akt2 independent of the transcription factors FoxA2, FoxO1, and SREBP1c. Cell Metab. 14, 516–527.

Wang, J., Duncan, D., Shi, Z., and Zhang, B. (2013). Web-based GEne SeT AnaLysis toolkit (WebGestalt): update 2013. Nucleic Acids Res. 41, W77–W83.

Wang, Y., Viscarra, J., Kim, S.J., and Sul, H.S. (2015). Transcriptional regulation of hepatic lipogenesis. Nat. Rev. Mol. Cell Biol. 16, 678–689.

Weiner, J., Kranz, M., Kloting, N., Kunath, A., Steinhoff, K., Rijntjes, E., Kohrle, J., Zeisig, V., Hankir, M., Gebhardt, C., et al. (2016). Thyroid hormone status defines brown adipose tissue activity and browning of white adipose tissues in mice. Sci. Rep. 6, 38124.

Xue, R., Lynes, M.D., Dreyfuss, J.M., Shamsi, F., Schulz, T.J., Zhang, H., Huang, T.L., Townsend, K.L., Li, Y., Takahashi, H., et al. (2015). Clonal analyses and gene profiling identify genetic biomarkers of the thermogenic potential of human brown and white preadipocytes. Nat. Med. 21, 760–768.

Yang, D., Diraison, F., Beylot, M., Brunengraber, D.Z., Samols, M.A., Anderson, V.E., and Brunengraber, H. (1998). Assay of low deuterium enrichment of water by isotopic exchange with [U-13C3]acetone and gas chromatography-mass spectrometry. Anal. Biochem. 258, 315–321.

Yeh, W.J., Leahy, P., and Freake, H.C. (1993). Regulation of brown adipose tissue lipogenesis by thyroid hormone and the sympathetic nervous system. Am. J. Physiol. 265, E252–E258.

Yoneshiro, T., Aita, S., Mastushita, M., Ogawa, T., Okamatsu-Ogura, Y., Kawai, Y., and Saito, M. (2011a). Age-related decrease in brown adipose tissue and obesity in humans. Obesity 19, S79.

Yoneshiro, T., Aita, S., Matsushita, M., Kameya, T., Nakada, K., Kawai, Y., and Saito, M. (2011b). Brown adipose tissue, whole-body energy expenditure, and thermogenesis in healthy adult men. Obesity 19, 13–16.

Yoneshiro, T., Aita, S., Matsushita, M., Kayahara, T., Kameya, T., Kawai, Y., Iwanaga, T., and Saito, M. (2013). Recruited brown adipose tissue as an anti-obesity agent in humans. J. Clin. Invest. 123, 3404–3408.

Yore, M.M., Syed, I., Moraes-Vieira, P.M., Zhang, T., Herman, M.A., Homan, E.A., Patel, R.T., Lee, J., Chen, S., Peroni, O.D., et al. (2014). Discovery of a class of endogenous mammalian lipids with anti-diabetic and anti-inflammatory effects. Cell 159, 318–332.

Yoshida, T., Yoshioka, K., Hiraoka, N., Umekawa, T., Sakane, N., and Kondo, M. (1994). Effect of CL 316,243, a novel beta 3-adrenoceptor agonist, on insulin secretion in perfused mouse pancreas. Endocr. J. 41, 671–675.

Yu, X.X., Lewin, D.A., Forrest, W., and Adams, S.H. (2002). Cold elicits the simultaneous induction of fatty acid synthesis and beta-oxidation in murine brown adipose tissue: prediction from differential gene expression and confirmation in vivo. FASEB J. 16, 155–168.

Zhao, S., Torres, A., Henry, R.A., Trefely, S., Wallace, M., Lee, J.V., Carrer, A., Sengupta, A., Campbell, S.L., Kuo, Y.M., et al. (2016). ATP-citrate lyase controls a glucose-to-acetate metabolic switch. Cell Rep. 17, 1037–1052.

STAR★METHODS

KEY RESOURCES TABLE

REAGENT or RESOURCE	SOURCE	IDENTIFIER
Antibodies		
Raptor	CST	Cat# 2280, RRID:AB_561245
ACL	CST	Cat# 4332, RRID:AB_2223744
ACSS2	CST	Cat# 3658S, RRID:AB_2222710
ACC	CST	Cat# 3676, RRID:AB_2219397
FAS	CST	Cat# 3180S, RRID:AB_2100796
UCP1	Abcam	Cat# ab10983, RRID:AB_2241462
ACETYL-LYS	CST	Cat# 9441, RRID:AB_331805
AKT1	CST	Cat# 2938, RRID:AB_915788
AKT2	CST	Cat# 3063, RRID:AB_2225186
TUBULIN	CST	Cat# 2125, RRID:AB_2619646
T308-AKT	CST	Cat# 4056, RRID:AB_331163
S473-Akt	CST	Cat# 4058, RRID:AB_331168
S473-AKT1	CST	Cat# 9018, RRID:AB_2629283
S474-AKT2	CST	Cat# 8599, RRID:AB_2630347
T246-PRAS40	CST	Cat# 2997S, RRID:AB_2258110
PRAS40	CST	Cat# 2691S, RRID:AB_2225033
T642-AS160	CST	Cat# 4288, RRID:AB_10545274
AS160	MILLIPORE	Cat# 07-741, RRID:AB_492639
MITO OXPHOS	Abcam	Cat# ab110413, RRID:AB_2629281
CHREBP	Novus Biologicals	NB400-135, Lot M5
SREBP1	EMD Millipore	Cat# 04-469, RRID:AB_612072
GLUT1	Abcam	Cat# ab652, RRID:AB_305540
GLUT4	CST	Cat# 2213, RRID:AB_823508
HA-Taq	CST	Cat# 2367S, RRID:AB_10691311
TH	Millipore	Cat# MAB318, RRID:AB_2201528
S563-HSL	CST	Cat# 4139, RRID:AB_2135495
S565-HSL	CST	Cat# 4137, RRID:AB_2135498
S660-HSL	CST	Cat# 4126, RRID:AB_490997
HSL	CST	Cat# 4107, RRID:AB_2296900
Perilipin	CST	Cat# 9349S, RRID:AB_10621999
S522-Perilipin	Vala	Cat# 4856
Mouse IgG	CST	Cat# 7076, RRID:AB_330924
Rabbit IgG	CST	Cat# 7074, RRID:AB_2099233
Biological Samples		
Supraclavicular BAT samples	Jespersen et al., 2013	N/A
Chemicals, Peptides, and Recombinant Proteins		
D20	Sigma	151882
4-hydroxy Tamoxifen	Toronto research chemicals	H954729
Tamoxifen	Sigma	T5648
T3	Sigma	T2877
Insulin	Sigma	I2643
IBMX	Sigma	I5879
Dexamethasone	Sigma	D1756

(Continued on next page)

Continued

REAGENT or RESOURCE	SOURCE	IDENTIFIER
Indomethacin	Sigma	I7378
HumulinR	Novolin	U-100
[1-14C]-2-bromopalmitic acid	Moravek	MC452
[1,2-3H]-deoxy-D-glucose	Perkin Elmer	NET328A001MC
D-[U-14C]-glucose	Perkin Elmer	NEC042V250UC
Critical Commercial Assays		
High Capacity cDNA reverse transcription kit	Applied Biosystems	4368813
RNeasy kit	Qiagen	74106
Deposited Data		
Gene expression	GEO	GSE96681
Experimental Models: Cell Lines		
UBC-Cre;Akt2floxed	This paper	N/A
UBC-Cre;Akt1/2 floxed	This paper	N/A
Experimental Models: Organisms/Strains		
Mouse: Akt1 floxed	Morrie Birnbaum lab	Wan et al., 2012
Mouse: Akt2 floxed	Morrie Birnbaum lab	Wan et al., 2011
Mouse: AG4Ox	Barbara Kahn lab	Shepherd et al., 1993
Mouse: Ucp1-CreER	Christian Wolfrum lab	Rosenwald et al., 2013
Mouse: B6.FVB-Tg(Ucp1-cre)1Evdr/J	Jackson labs	024670
Mouse: C57BL/6J	Jackson labs	000664
Mouse: B6.129(Cg)-Gt(ROSA)26Sortm4(ACTB-tdTomato,-EGFP)Luo/J	Jackson labs	007676
Mouse: B6;FVB-Tg(Adipoq-cre)1Evdr/J	Jackson labs	010803
Mouse: B6.Cg-Tg(UBC-cre/ERT2)1Ejb/2J	Jackson labs	008085
Oligonucleotides		
Mouse primers	IDT	See Table S3
Human primers	IDT	See Table S4
Human Taqman assays	ThermoFisher	See Table S4
Recombinant DNA		
ChREBPalpha	Schupp lab	N/A
ChREBPbeta	Schupp lab	N/A
nSREBP1c	This paper	N/A
Glut1	This paper	N/A
Software and Algorithms		
Graphpad	GraphPad Software	Graphpad.com
Adobe Illustrator	Adobe	Adobe.com
TreeView 1.1	Java TreeView	http://jtreeview.sourceforge.net
Morpheus	Broad Institute	https://software.broadinstitute.org/morpheus/
FLIR Tools version 2.1	FLIR systems	FLIR.com
Other		
Rodent incubators	Powers Scientific	RIT33SD
Infrared thermal camera (FLIR T420)	FLIR	T420
Rectal thermometer probe	Braintree Scientific Inc.	Microtherma 2 system

CONTACT FOR REAGENT AND RESOURCE SHARING

Further information and request for resources and reagents should be directed to and will be fulfilled by the Lead Contact, David A Guertin (david.guertin@umassmed.edu).

EXPERIMENTAL MODEL AND SUBJECT DETAILS

Mice and Mice Housing

C57BL/6J mice (JAX stock 000664), R26R-mTmG mice (JAX stock 007676), Ucp1-CreER mice were described before (Rosenwald et al., 2013), UCP1-Cre (JAX stock 024670), adiponectin-Cre (JAX stock 010803).

Husbandry Conditions

Mice were housed in the Animal Medicine facilities of the UMMS in a clean room set at 22°C and 45% humidity under daily 12h light/dark cycles in ventilated racks with cages changed every two weeks. For the four weeks temperature acclimation experiments, mice were simultaneously housed in two rodent incubators (RIT33SD, Powers Scientific) within the Animal Medicine facilities of the UMMS. One of them had the temperature adjusted to 30°C (thermoneutrality group). Another incubator had its temperature decreased by four degrees weekly until reaching 6°C at which temperature the mice stayed for a week (severe cold group). Room temperature group mice were co-housed in the same facility as the mice in rodent incubators. Mouse cages were changed weekly using components pre-adjusted to temperature. No cage enrichment was used in this set of experiments.

Wildtype C57BL/6J mice were started in temperature acclimation experiments at 10 weeks old and sac at 14 weeks old. In the case of inducible knockout mice in temperature acclimation experiments, mice were treated with tamoxifen at 6 weeks of age and waited until 9 or 11 weeks of age to start the 4 or 2 weeks of temperature treatment, respectively. All inducible mice in temperature acclimation experiments were sac at 13 weeks of age.

All animals used here were males in C57BL/6J background. Age of sacrificed ranges from 9-25 weeks old depending on the experiment. Please see figure legend for specific age and number of mice used.

All animal experiments were approved by the University of Massachusetts Medical School Institutional Animal Care and Use Committee.

Cell Culture

Brown preadipocytes were isolated from *Ubc-Cre^{ERT2};Akt1^{floxed}Akt2^{floxed}* or *Ubc-Cre^{ERT2}; Akt2^{floxed}* P1 neonates and immortalized with pBabe-SV40 Large T. The gender of neonates was not determined. Cells were maintained in high-glucose DMEM in incubators at 37°C and 5% CO_2. Cells stably expressing recombinant proteins were obtained by using a lentiviral system. For brown adipocyte differentiation, cells were seeded at medium density and allowed to proliferate to confluence in the presence of high-glucose DMEM including 10% FBS, 1% antibiotics, 20nM insulin and 1nM T_3. After 4 days, cells were induced to differentiate by adding induction media (high-glucose DMEM including 10% FBS, 1% antibiotics, insulin 20nM, 1nM T_3, 0.125mM indomethacin, 2 μg/mL dexamethasone and 0.5mM 3-isobutyl-1-methylxanthine (IBMX)) for 2 days. After this, the medium (high-glucose DMEM including 10% FBS and 1% antibiotics) with insulin and T_3 was changed every 2 days until day 12. Deletion of *Akt1* and/or *Akt2* was achieved by treating the cells with one dose of 4-hydroxytamoxifen (4-OHT, 1μM) at day 8 of differentiation. Control cells received equivalent volume of ethanol (vehicle). To analyze insulin signaling and glucose uptake, cells were serum starved (in high-glucose DMEM) for 3 hr and insulin was added for 15 min. For all other experiments, fresh media (high-glucose DMEM including 10% FBS, 1% antibiotics, 20nM insulin and 1nM T_3) was added to the cells one hr before harvest.

Human BAT

Supraclavicular BAT samples from patients under suspicion of cancer in the neck and head area, aged 22-84 (50% of males), originated from a previous study (Jespersen et al., 2013). The study protocol was approved by The Scientific-Ethics Committees of the Capital Region and of Copenhagen and Frederiksberg Municipalities, Denmark, (journal number H-A-2009-020 and H-17014258) and the study was performed in accordance with the Helsinki declaration.

METHOD DETAILS

Tissue Dissection

Tissues were carefully dissected to avoid surrounding tissue contamination. Adipose tissue notation used here was described previously (Sanchez-Gurmaches and Guertin, 2014). BAT depots: interscapular BAT (iBAT), subscapular BAT (sBAT), cervical BAT (cBAT), periaortic BAT(paBAT), perirenal BAT (prBAT); subcutaneous WAT depots: anterior subcutaneous WAT (asWAT), posterior subcutaneous WAT (also called inguinal, psWAT); visceral WAT depots: mesenteric WAT (mWAT), retroperitoneal WAT (rWAT), perigonadal WAT (pgWAT). Mice were dissected at early morning without fasting or any other alteration, unless noted in the figure legend.

Tamoxifen Treatment

Tamoxifen was dissolved in corn oil/ethanol (9:1 vol/vol) at 2mg/mL by shaking at 4°C overnight. 6 week old mice were I.P. injected with 2mg/day/mouse for 5 times in a period of seven days.

Acute/Prolong Cold Challenge

9 weeks old *Akt2^{ucp1ER}* mice (3 weeks after tamoxifen treatment) were placed at 4°C early in the morning of the experiment in overnight pre-chilled caging with free access to pre-chilled food and water. In another set of experiments, animals were placed in a pre-acclimated 6°C chamber for two weeks.

Fasting/Refeeding
Overnight fasted 9 weeks old mice, were refed by adding food to their cages for 45 min before dissection.

High Fat Diet Feeding
Male mice aged 9 weeks were fed 60% HFD (D12492 Harlan laboratories) or normal chow diet (Prolab Isopro RMH 3000) for either 2 or 12 weeks. Food intake and body weight was monitored weekly. Tissues were harvested upon termination of the experiment.

Temperature Measurements
Internal temperature was recorded by using a rectal thermometer probe (Microtherma 2 system, Braintree Scientific). BAT and tail temperatures were obtained using an infrared thermal camera (FLIR T420) in lightly anesthetized mice and analyzed with FLIR tools.

Glucose and Insulin Tolerance Tests
Overnight fasted mice were injected with glucose at 2 gKg^{-1} of body weight by i.p. injection. Insulin injection (HumulinR) was done in 6 hr fast mice at 0.75 UKg^{-1} of body weight by i.p. injection. Blood glucose was measured by tail bleeding using a commercial blood glucose tester.

In Vivo Glucose and FA Uptake
Animals were fasted for 6 hr to eliminate confounding effects of hormones and food. In the afternoon, mice were i.p. injected with 150 μL of 4% fatty acid free-BSA PBS containing 10 μCi of [1-^{14}C]-2-bromopalmitic acid and 10 μCi of [1,2-^{3}H]-deoxy-D-glucose. After two hr, mice were sacrificed and tissues dissected. Tissues were lysed in PBS using a TissueLyzer (Qiagen) and radioactivity was measure in whole lysate (without previous centrifugation). Results were normalized to tissue weight.

Tissue Histology
Tissue pieces were fixed in 10% formalin. Embedding, sectioning and Hematoxylin and Eosin (H&E) staining was done by the UMMS Morphological Core facility.

Metabolite Profiling
Polar and non-polar metabolites were analyzed at the Whitehead Institute Metabolite Profiling Core Facility.

Brown fat samples were homogenized in four volumes of water using a TissueLyser II (Qiagen) and profiles of polar metabolites and lipids were obtained using LC-MS. The polar metabolite profiling methods were developed using reference standards of each metabolite to determine chromatographic retention times and MS multiple reaction monitoring transitions, declustering potentials and collision energies. Lipid profiling data were acquired in full scan mode and lipids were identified on the basis of mass to charge ratio and retention time. The three LC-MS methods have been recently described (Townsend et al., 2013). Briefly, negative ionization mode data were acquired using an ACQUITY UPLC (Waters) coupled to a 5500 QTRAP triple quadrupole mass spectrometer (AB SCIEX) running hydrophilic interaction chromatography (HILIC) method. A 30μL aliquot of each homogenate was extracted using 120 μL of 80% methanol (VWR) containing 0.05 ng/μL inosine-15N4, 0.05 ng/μL thymine-d4, and 0.1 ng/μL glycocholate-d4 as internal standards (Cambridge Isotope Laboratories). The samples were centrifuged (10 min, 9,000 x g, 4°C) and the supernatants (10 μL) were injected directly onto a 150 x 2.0 mm Luna NH2 column (Phenomenex) that was eluted at a flow rate of 400 μL/min. Initial mobile phase conditions were 10% mobile phase A (20 mM ammonium acetate and 20 mM ammonium hydroxide (Sigma-Aldrich) in water (VWR)) and 90% mobile phase B (10 mM ammonium hydroxide in 75:25 v/v acetonitrile/methanol (VWR)) and the column was eluted using a 10 min linear gradient to 100% mobile phase A. The ion spray voltage was -4.5 kV and the source temperature was 500°C.

Positive ionization mode data were acquired using an 1100 Series pump (Agilent) and an HTS PAL autosampler (Leap Technologies) coupled to a 4000 QTRAP triple quadrupole mass spectrometer (AB SCIEX). A 10μL aliquot of each homogenate was extracted using nine volumes of 74.9:24.9:0.2 (v/v/v) acetonitrile/methanol/formic acid containing stable isotope-labeled internal standards (0.2 ng/μL valine-d8, Isotec; and 0.2 ng/μL phenylalanine-d8 (Cambridge Isotope Laboratories)). Samples were centrifuged (10 min, 9,000 x g, 4°C) and supernatants (10 μL) were injected onto a 150 x 2.1 mm Atlantis HILIC column (Waters). The column was eluted isocratically at a flow rate of 250 μL/min with 5% mobile phase A (10 mM ammonium formate and 0.1% formic acid in water) for 1 min followed by a linear gradient to 40% mobile phase B (acetonitrile with 0.1% formic acid) over 10 min. The ion spray voltage was 4.5 kV and the source temperature was 450°C.

For lipid analyses, a 10μL aliquot of each homogenate was extracted with 190μL of isopropanol containing 0.25 ng/μL 1-dodecanoyl-2-tridecanoyl-sn-glycero-3-phosphocholine (Avanti Polar Lipids). After centrifugation, supernatants (10 μL) were injected directly onto a 150 x 3.0 mm Prosphere HP C4 column (Grace). The column was eluted isocratically with 80% mobile phase A (95:5:0.1 vol/vol/vol 10mM ammonium acetate/methanol/acetic acid) for 2 min followed by a linear gradient to 80% mobile-phase B (99.9:0.1 vol/vol methanol/acetic acid) over 1 min, a linear gradient to 100% mobile phase B over 12 min, then 10 min at 100% mobile-phase B. MS analyses were carried out using electrospray ionization and Q1 scanning in the positive ion mode. The ion spray voltage was 5.0 kV and the source temperature was 400°C.

MultiQuant 1.2 software (AB SCIEX) was used for automated peak integration and metabolite peaks were manually reviewed for quality of integration and compared against a known standard to confirm identity.

To minimize artefacts due to possible changes in the state of the instrument between the beginning and end of the LC/MS batch, group biological replicates were interspersed and re-grouped for data analysis. The area of each lipid species peak was normalized to the total lipid signal to reflect the actual LC/MS injected lipid amount per sample represented as Area/Total Lipid Area).

Gene Expression and Western Blot Analysis
For western blot analysis protein lysates (typically 10μg per lane) were run in SDS acrylamide/bis-acrylamide gels (typically 10%), transferred to PVDF membranes and detected with specific antibodies as specified in Table S2.

Total RNA was isolated using Qiazol (Qiagen) and RNeasy kit (Qiagen), retrotranscription was done using High Capacity cDNA reverse transcription kit (#4368813, Applied Biosystems) and analyzed in a StepOnePlus real-time PCR machine. Primer sequences are shown in Table S3.

Whole Mount Confocal Microscopy
Small pieces of adipose tissues were mounted with Fluoromount-G (Southern Biotech) and imaged in a LSM 5 Pascal (Zeiss) point scanner confocal system using a 40x oil immersion objective. eGFP was excited at 488 nm and detected from 515 to 565 nm. tdTomato was excited at 543 nm and detected from 575 to 640 nm.

Gene Expression Profile
Input Data
Four replicates for three different temperature conditions (severe cold, room temperature and thermoneutrality) were sequenced resulting in twelve single-end fastq sequences of 40bp read length. Four replicates for two genotypes (wildtype and AKT2 knockout) for two different temperature conditions (room and thermoneutrality) were also sequenced resulting in sixteen single-end fastq sequences of 40bp to 50bp read length.

RNA-Seq Data Analysis
The fastq files were checked for quality control using FastQC (version 0.10.1) (http://www.bioinformatics.babraham.ac.uk/projects/fastqc) and subsequently aligned against the mouse reference genome (Ensembl GRCm38) using the aligner STAR (version 2.4.2a) (Dobin et al., 2013). Gene expression quantification was done with STAR (using the –quantMode GeneCounts option) to generate uniquely mapped read counts at the gene level. Differential expression analysis was performed with edgeR (version 3.14.0) (Robinson et al., 2010) using the count matrix as input. HTSFilter was used to filter out constant level of low counts from pairwise conditions (Rau et al., 2013). Tables of significantly differentially expressed genes with padj threshold of 0.05 were generated for further analysis. Functional enrichment analysis was done using the online web tools at WebGestalt (Wang et al., 2013).

GEO accession number GSE96681.

In Vivo Lipogenesis Assay
D20 labeling
Three days prior to termination, mice were intraperitoneally injected with 0.035 mL/g body weight 0.9% NaCL D2O (Sigma, 151882) and drinking water was replaced with 8% D2O enriched water.

Plasma D2O Enrichment
The 2H labeling of water from samples or standards was determined via deuterium acetone exchange (McCabe et al., 2006; Yang et al., 1998). 5 uL of sample or standard was reacted with 4 uL of 10N NaOH and 4 uL of a 5% (v/v) solution of acetone in acetonitrile for 24 hr. Acetone was extracted by the addition of 600 uL chloroform and 0.5 g Na2SO4 followed by vigorous mixing. 100 uL of the chloroform was then transferred to a GCMS vial. Acetone was measured using an agilent DB-35MS column (30 m 3 0.25mm i.d. 3 0.25 mm, Agilent J&W Scientific) installed in an Agilent 7890A gas chromatograph (GC) interfaced with an Agilent 5975C mass spectrometer (MS) with the following temperature program: 60°C initial, increase by 20°C/min to 100°C, increase by 50°C/min to 220°C, and hold for 1 min. The split ratio was 40:1 with a helium flow of 1 mL/min. Acetone eluted at approximately 1.5min. The mass spectrometer was operated in the electron impact mode (70 eV). The mass ions 58 and 59 were integrated and the % M1 (m/z 59) calculated. Known standards were used to generate a standard curve and plasma % enrichment was determined from this. All samples were analyzed in triplicate.

Total fatty acids were extracted from tissues and plasma using a bligh and dyer based methanol/chloroform/water extraction with C16 D31 as an internal standard. Briefly, 500 uL MeOH, 500 uL CHCL3, 200 uL H2O and fatty acid isotope internal standards were added to weighed pre-ground tissue. This was vortexed for 10 min followed by centrifugation at 10,000 g for 5 min. The lower chloroform phase was dried and then derivitised to form fatty acid methyl esters via addition of 500 uL 2% H2SO4 and incubation at 50°C for 2 hr. FAMES were extracted via addition of 100 uL saturated salt solution and 500 uL hexane and these were analyzed using a Select FAME column (100m x 0.25mm i.d.) installed in an Aglient 7890A GC interfaced with an Agilent 5975C MS using the following temperature program: : 80°C initial, increase by 20°C/min to 170°C, increase by 1°C/min to 204°C, then 20°C/min to 250°C and hold for 10 min.

Calculations
The % mass isotopomer distributions of each fatty acid was determined and corrected for natural abundance using in-house algorithms adapted from Fernandez et al. (Fernandez et al., 1996). Calculation of the fraction of newly synthesized fatty acids (FNS) was based on the method described by Lee et al. (Lee et al., 1994), where FNS is described by the following equation:

$$FNS = ME/(n \times p)$$

Where ME is the average number of deuterium atoms incorporated per molecule(ME =1 x m1 + 2 x m2 +3 x m3…), p is the deuterium enrichment in water and n is the maximum number of hydrogen atoms from water incorporated per molecule. N was determined using the equation:

$$m2/m1 = (N-1) /2 \times p/q$$

As described by Lee et al (Lee et al., 1994) where q is the fraction of hydrogen atoms and p + q = 1. The molar amount of newly synthesized fatty acids was determined by:

$$MNS = FNS \times total\ fatty\ acid\ amount\ (nmoles/mg\ tissue).$$

In Vitro Lipogenesis Assay

Lipogenesis activity was analyzed in differentiated brown adipocytes in vitro as previously reported (Tang et al., 2016). Differentiated brown adipocytes were incubated in Krebs Ringer Hepes (KRH) buffer supplemented with 2.5% fatty acid free-BSA and 2uCi/mL D-[U-^{14}C]-glucose (PerkinElmer) for 4.5 hr with or without the presence of 150nM insulin. The cells were lysed with Doley's solution (isopropyl alcohol:hexane:1N H_2SO_4 (v:v:v) =4:1:1), and newly synthesize lipids were extracted with hexane. The hexane phase was evaporated, reconstituted in scintillation fluid and radioactivity measured.

Human Brown Fat Analysis

Supraclavicular BAT samples originated from a previous study (Jespersen et al., 2013). Briefly, participants were included prior to elective surgery due to suspicion of cancer in the neck area, via the outpatient clinic at the Department of Oto-Rhino-Laryngology Head & Neck Surgery at Rigshospitalet. All participants provided written consent before enrollment. Biopsies were obtained during surgery by an experienced surgeon. Tissue was removed using scalpel and scissor. Immediately after removal samples were flash frozen in liquid nitrogen before being stored on – 80° C until analyses were performed. Due to large variation in *UCP1* expression, supraclavicular samples were divided into a BAT high and a BAT low group based on UCP1 mRNA expression, n = 10 and n=9 respectively. The study protocol was approved by The Scientific-Ethics Committees of the Capital Region and of Copenhagen and Frederiksberg Municipalities, Denmark, (journal number H-A-2009-020 and H-17014258) and the study was performed in accordance with the Helsinki declaration.

Total RNA isolation from adipose tissue biopsies was performed using TRizol reagent according to the manufacture's protocol. RNA was dissolved in nuclease-free water and quantified using a Nanodrop ND 1000 (Saveen Biotech). Total RNA (0.25μg) was reverse-transcribed using the High Capacity cDNA Reverse Transcription Kit (Applied Biosystems). cDNA samples were loaded in triplicate and qPCR was performed using real-time quantitative PCR, using the ViiA^{tm} 7 platform (Applied Biosystems). Table S4 included the primers and Taq-assays used.

QUANTIFICATION AND STATISTICAL ANALYSIS

Data are presented as mean + SEM, unless stated otherwise. Student's t test or analysis of variance (one or two ways), as appropriate, were used to determine statistical significance. For human data, Mann-Whitney test and linear regression were used. Because lipid species does not follow a normal distribution, the Wilcoxon test within GraphPad Prism was used for statistical significance. No pre-test was used to choose sample size. Statistical analysis was done using GraphPad Prism except for global RNA expression (see Method Details). Heatmaps were plotted using TreeView 1.1 or Morpheus (Broad Institute). The number of mice used per experiment is stated in each figure legend.

DATA AND SOFTWARE AVAILABILITY

Whole genome expression profiles are available at GEO accession number GSE96681.